

On the Validity of Dark Matter Effective Theory

Martin Bauer,¹ Anja Butter,¹ Nishita Desai,² J. Gonzalez-Fraile,¹ and Tilman Plehn¹

¹*Institut für Theoretische Physik, Universität Heidelberg, Germany*

²*Laboratoire Charles Coulomb (L2C) & Laboratoire Univers et Particules
de Montpellier (LUPM), CNRS-Université de Montpellier, France*

An effective theory of dark matter offers an attractive framework for global analyses of dark matter. In the light of global fits we test the validity of the link between the non-relativistic dark matter annihilation, or the predicted relic density, and LHC signatures. Specifically, we study how well the effective theory describes the main features of simple models with s-channel and t-channel mediators coupling to the Standard Model at tree level or through one-loop diagrams. Our results indicate that global dark matter analyses in terms of effective Lagrangians are highly non-trivial to interpret in term of actual models.

CONTENTS

I. Introduction	2
Effective Lagrangian for LHC	3
Simplified models	3
II. Tree-level scalar in t-channel	5
Total rate	7
Kinematic distributions	8
Effective Lagrangian vs model	10
III. Tree-level vector in s-channel	11
Total rate	13
Kinematic distributions	15
Effective Lagrangian vs model	15
Axial-vector case	16
IV. Loop-mediated scalar in s-channel	18
Total rate	19
Kinematic distributions	23
Effective Lagrangian vs model	23
V. Loop-mediated scalar in t-channel	24
Total rate	24
Effective Lagrangian vs model	26
VI. Summary	27
A. Detector effects	29
References	31

I. INTRODUCTION

An effective field theory [1, 2] of dark matter can systematically describe the effects of heavy, non-propagating mediators between the dark sector and the Standard Model. In particular for light dark matter with $m_\chi \lesssim v$, an effective Lagrangian can describe the effects of heavier mediators [3–5], always assuming

$$m_{\text{med}} > m_\chi . \quad (1)$$

The corresponding effective Lagrangian then includes a new physics scale $\Lambda \sim m_{\text{med}}$ and the corresponding coupling g . This description is generally accepted for processes with a low external energy scale and provided the effective Lagrangian expansion does not interfere with the velocity suppression. This includes dark matter annihilation in the early universe [4, 6], dark matter annihilation with decay products observed today [7], or direct dark matter searches based on scattering with nuclei [3, 8]. Issues with this picture occur for dark matter production at the LHC [9]. In this paper we attempt a comprehensive, quantitative study of the limitations of an effective theory of dark matter.

The main question is *if an effective theory can be used to link very different observations as part of a global dark matter analysis, and if in this link it correctly represents the patterns of a full model behind it*. From detailed studies of effective theories in the Higgs sector at the LHC [10] we know that simple arguments based on dimensional analysis and scale estimates [11, 12] are not always well-suited for LHC physics. Instead, we should establish the (non-)applicability of effective theory approximations model-by-model and observable-by-observable [13–16]. Obviously, we will focus on standard LHC processes as the limiting factors. We will study mono-jet or related signatures, where the relevant observables are the transverse momentum distribution of the missing particles recoiling against one or more jets and, to some degree, the total rate. The only additional ingredient we will use is the relic density as a rough guideline if our model for the dark sector could be responsible for the observed dark matter density [4, 5].

All models in our study will include simple dark matter sectors, allowing for a straightforward test if an observed missing energy signal is likely to be related to the dark matter relic density in our universe. The reasoning behind this link is that from a practical perspective the LHC either adds some relevant piece of information to a global dark matter analysis — or the question if the LHC observable is well described by the effective Lagrangian is irrelevant*. To get an idea what kind of thermal dark matter signal we would be looking for at the LHC, we can estimate the observed relic density, for example assuming the usual $2 \rightarrow 2$ annihilation process mediated by a dimension-6 operator

$$\langle \sigma_{\text{ann}} v \rangle \propto \frac{g^4 E^2}{4\pi m_{\text{med}}^4} \sim \frac{g^4 m_\chi^2}{4\pi m_{\text{med}}^4} . \quad (2)$$

We will at least roughly let the observed relic density guide us through the dark sector’s parameter space. Typically, the above scaling gives us a lower limit on the ratio m_χ/m_{med}^2 , an upper limit on the mediator mass, or a lower limit on LHC production cross sections. The rough relation between the mediator and dark matter masses is

$$\begin{aligned} \frac{m_{\text{med}}^2}{g^2 m_\chi} = 8 \text{ TeV} \quad m_\chi \stackrel{=10 \text{ GeV}}{\Rightarrow} \quad \frac{m_{\text{med}}}{g} = 150 \text{ GeV} \\ m_\chi \stackrel{=m_{\text{med}}/2}{\Rightarrow} \quad \frac{m_{\text{med}}}{g} = 2 \text{ TeV} . \end{aligned} \quad (3)$$

* To search for missing transverse momentum at the LHC neither requires a well-defined model framework nor an effective theory justification.

In this simple model the dark matter agent can be very light, but the mediator will typically be heavy. For weakly interacting models the appropriate dark matter and mediator mass scales will decrease. Similarly, if we only require our dark matter agent to be responsible for part of the observed relic density, the annihilation cross section can be larger, or the mass scales can be (slightly) smaller.

Just as a side remark, for an s -channel mediator with the pole condition $m_{\text{med}} = 2m_\chi$ the annihilation rate scales like $g^4 m_\chi^2 / (m_{\text{med}}^2 \Gamma_{\text{med}}^2)$, introducing the width as an additional scale and strongly reducing the required couplings. We will not follow this well-known path in Higgs portal scenarios and instead study generic $2 \rightarrow 2$ annihilation processes.

Effective Lagrangian for LHC

Additional external energy scales are introduced by the hadron collider environment of a given dark matter process, now leading to three relevant energy scales

$$\{ m_\chi, m_{\text{med}}, \sqrt{s} \} . \quad (4)$$

For dark matter annihilation, indirect detection, and direct detection these additional energy scales are no challenge to the validity of the effective theory. At the LHC the situation is less obvious, because kinematic cuts or a potential kinematic link between the mediator mass m_{med} and the energy transfer can push the momentum transfer of the process to energy scales $\sqrt{s} > m_\chi$. One promising, general dark matter search targets jet production with a pair of dark matter particles. The key observables here are the \cancel{E}_T and $p_{T,j}$ distributions. For simple hard processes the two transverse momentum distributions are rapidly dropping and strongly correlated. They define the relevant energy scales

$$\{ m_\chi, m_{\text{med}}, \cancel{E}_T^{\text{min}} \} . \quad (5)$$

The experimentally relevant \cancel{E}_T or $p_{T,j}$ regime is given by a combination of the signal mass scale, the kinematics of the dominant $Z_{\nu\nu} + \text{jets}$ background, and triggering. Our effective theory has to reproduce two key observables,

$$\sigma_{\text{tot}}(m_\chi, m_{\text{med}}) \Big|_{\text{acceptance}} \quad \text{and} \quad \frac{d\sigma(m_\chi, m_{\text{med}})}{d\cancel{E}_T} \sim \frac{d\sigma(m_\chi, m_{\text{med}})}{dp_{T,j}} , \quad (6)$$

the latter over the relevant phase space regime. These two LHC observables will guide us through the different models in our study.

Finally, the hadronic LHC energy of 13 TeV, combined with reasonable parton momentum fractions defines an absolute upper limit, above which for example a particle in the s -channel cannot be produced as a propagating state. This adds another energy scale to our setup,

$$\{ m_\chi, m_{\text{med}}, \cancel{E}_T^{\text{min}}, \sqrt{s_{\text{max}}} \} . \quad (7)$$

These four scales define the framework of our effective theory considerations at the LHC.

Simplified models

As described above, any effective theory description of dark matter relies on some fundamental assumptions on the new physics spectrum. For example, if the hierarchy in Eq.(1) is inverted,

$$m_{\text{med}} < m_\chi , \quad (8)$$

the effective theory is often not applicable. We can instead describe dark matter annihilation and production through a simplified model with a dynamic mediator field [16, 17]. The relic density becomes largely independent of the light mediator mass, and the usual WIMP condition gives the dark matter mass through

$$\langle\sigma_{\text{ann}}v\rangle\sim\frac{g^4}{4\pi m_\chi^2}\quad\Rightarrow\quad\frac{m_\chi}{g^2}\sim 4\text{ TeV} . \quad (9)$$

The phenomenology of such a model can be illustrated with the Higgs portal story: the light mediator will be produced directly, and it will decay to two light Standard Model states through its production coupling. A decay to two dark matter agents will only occur for off-shell mediator production and will be strongly suppressed. In other words, the LHC we will look for light new resonances, and this signature will not allow us to identify the mediator nature of this state or say anything about dark matter.

In terms of LHC energy scales this situation reads more specifically

$$m_{\text{med}}<\sqrt{s_{\text{max}}}, m_\chi . \quad (10)$$

The mediator appears as the propagating degree of freedom at the LHC. The spin and quantum numbers of the mediator states play a significant role; vector mediators can couple to light quarks [18], while scalar mediators typically couple to top quarks [19–21]. Sizeable light-quark couplings of scalar mediators in the s -channel are strongly constrained by flavor physics [22]. Realistic scalar mediators arise from mixing with the SM Higgs [23]. This scenario is strongly constrained by Higgs physics, but allows for an electroweak mono-jet signal comparable in size to the QCD-induced mono-jet signal [24]. Colored scalar mediators with t -channel interactions can have large, flavor-specific couplings, because the mediator is a triplet in flavor space [25].

While at the LHC the search for jets plus missing energy — or mono-jet signatures — is fully established, the nature of mediators can also be studied in a variety of mono- X final states ($X = \gamma, Z, W$). These rates are typically at least an order of magnitude smaller than mono-jet cross-sections. However, for gluon or photon radiation the up-type and down-type quark initial states do not interfere, and the sign of the relative couplings are irrelevant. In contrast, the mono- W signature with opposite-sign couplings to up-type and down-type quarks can exceed the mono-jet signal for large transverse momenta [26]. This enhancement can be linked to an eventually unitarity-violating part of the amplitude [27]. A gauge-invariant implementation of such a model will be tamed by $Z - Z'$ mixing, or more general new physics through higher-dimensional operators. Similar, power-enhanced unitarity violation also exist in mono- Z and mono-Higgs signatures for vector mediators with axial-vector couplings [28]. A logarithmic divergence exists in mono- Z production mediated through scalar mediators at one loop [21]. However, aside from mono- W production, these divergences do not lead to actual problems at the LHC [29], and mono-jet searches are still the key search strategy for mediators at the LHC.

II. TREE-LEVEL SCALAR IN T-CHANNEL

One dark matter scenario, inspired for example by supersymmetry, is a fermionic dark matter candidate combined with a scalar mediator. The mediator \tilde{u} couples the dark matter fermion χ to an up-type quark, implying that it carries a color charge in the fundamental representation. Any model for such a t -channel mediator has to assume at least two interactions,

$$u - \tilde{u} - \chi \quad \text{dark matter annihilation} \quad \tilde{u} - \tilde{u} - g(-g) \quad \text{QCD} . \quad (11)$$

The first interaction has no structural counterpart in the Standard Model, so we are free to choose its size. In supersymmetric models it is fixed by the corresponding electroweak gauge or Yukawa couplings [30]. Because of this interaction the t -channel mediator always has to be heavier than then dark matter fermion,

$$m_{\tilde{u}} > m_{\chi} + m_q \approx m_{\chi} , \quad (12)$$

otherwise the dark matter agent decays. The second interaction occurs through the QCD part of the covariant derivative. The mediator will also have Z and γ interactions from the covariant derivative, but we assume them to be sub-leading at the LHC. In our very simple toy model the dark matter interaction is described by

$$\mathcal{L} \supset y_{\tilde{u}} (\bar{u}_R \chi) \tilde{u} + \text{h.c.} \quad (13)$$

We assume $y_{\tilde{u}} = 1$, unless the value is specified. Naively, the mono-jet production rate scales like $\sigma_{\cancel{E}T+j} \propto g_s^2 y_{\tilde{u}}^4$. The mediator width becomes [31]

$$\frac{\Gamma_{\tilde{u}}}{m_{\tilde{u}}} = \frac{y_{\tilde{u}}^2}{16\pi} \frac{(m_{\tilde{u}}^2 - m_{\chi}^2)^2}{m_{\tilde{u}}^4} < \frac{y_{\tilde{u}}^2}{16\pi} \lesssim 2\% . \quad (14)$$

As long as its coupling to SM fermions matches the flavor structure of the Standard Model, the t -channel mediator is a narrow resonance over our entire relevant parameter space.

From this Lagrangian we can compute the relic density using FEYNRULES [32] and MICROMEGAS [33]. In Fig. 1 we show the predicted relic density for different cuts in the two-dimensional dark matter vs mediator parameter space. In the left panel we see that for light dark matter the measured relic density requires a comparably light mediator within the reach of the LHC. The numbers are slightly different than in Eq.(3) because of the color factor N_c in the annihilation rate. In the second panel we see that for too heavy mediators there is no dark matter mass which predicts the correct relic density. This occurs because the required dark matter mass becomes too large, eventually exceeding the mediator mass and leading to dark matter decay channels. Finally, in the right panel we confirm the inverse quadratic scaling with a linked dark matter and mediator mass scale and the clear preference for ratios $m_{\tilde{u}} > m_{\chi}$. In essence, the observed relic density is in accordance with an effective theory description of the t -channel mediator model. Note that if we choose a smaller coupling, for example $y_{\tilde{u}} \lesssim 1/2$, the model will not give the correct relic density for parameter choices allowed by LHC. If the t -channel mediator only couples along the lines of the Standard Model flavor structure, additional mediators for example carrying lepton number can even dominate the dark matter annihilation rate.

At the LHC the t -channel mediator model has very distinct features, illustrated in Fig. 2. The two partonic processes:

$$u\bar{u} \rightarrow \chi\bar{\chi}g \quad \text{and} \quad ug \rightarrow \chi\bar{\chi}u \quad (15)$$

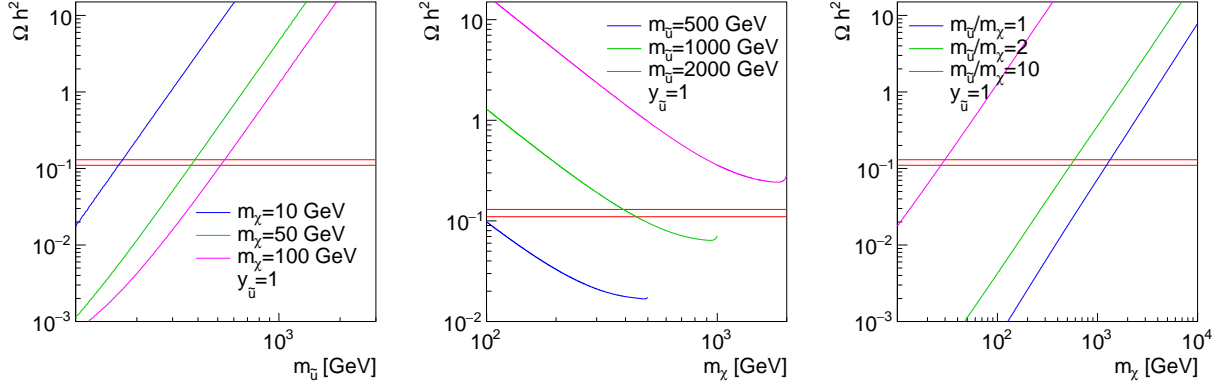


Figure 1. Relic density for the t -channel mediator model as a function of the mediator mass for constant dark matter mass (left), as a function of the dark matter mass for constant mediator mass (center) and as a function of the dark matter mass for a constant ratio of mediator to dark matter mass. We assume $y_{\tilde{u}} = 1$.

are of the same order in perturbation theory and experimentally indistinguishable. The second of these two processes can be dominated by an on-shell production of the mediator,

$$ug \rightarrow \chi \tilde{u} \rightarrow \chi (\bar{\chi} u). \quad (16)$$

As for the usual $2 \rightarrow 2$ annihilation process, we can cross this amplitude into an annihilation process, now describing the co-annihilation $\chi \tilde{u} \rightarrow ug$. The main difference between the (co-) annihilation and LHC interpretations of this amplitude is that in the prediction of the relic density it only contributes for $m_{\tilde{u}} \lesssim m_{\chi} + 10\%$, while at the LHC it dominates the mono-jet rates even for $m_{\tilde{u}} \gg m_{\chi}$. This challenges the theoretical link between LHC production and dark matter annihilation.

Finally, we can pair-produce the strongly interacting mediators through the third Feynman diagram in Fig. 2,

$$q\bar{q}/gg \xrightarrow{\text{QCD}} \tilde{u}\tilde{u}^* \xrightarrow{\text{dark matter}} (\bar{\chi} u)(\chi \bar{u}). \quad (17)$$

From many studies in the supersymmetry framework we know that for a wide range of mediator masses this pair production process completely dominates the $\chi\chi$ +jets process. If we can identify the $\chi\chi jj$ final state we can use the m_{T2} distribution to extract the masses of both the mediator and the dark matter candidate. On the other hand, the process is entirely QCD-mediated and the 100% branching fraction gives us no information about the $\bar{u} - \chi - \tilde{u}$ interaction. In other words, in the presence of this on-shell production process there is no link between LHC observables and dark matter properties of our t -channel (simplified) model.

For the pair-production process we can apply the search results for a single supersymmetric

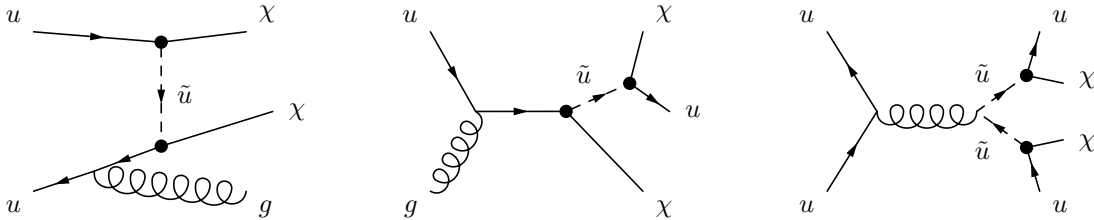


Figure 2. Feynman diagrams describing dark matter production in the t -channel mediator model defined in Eq.(13).

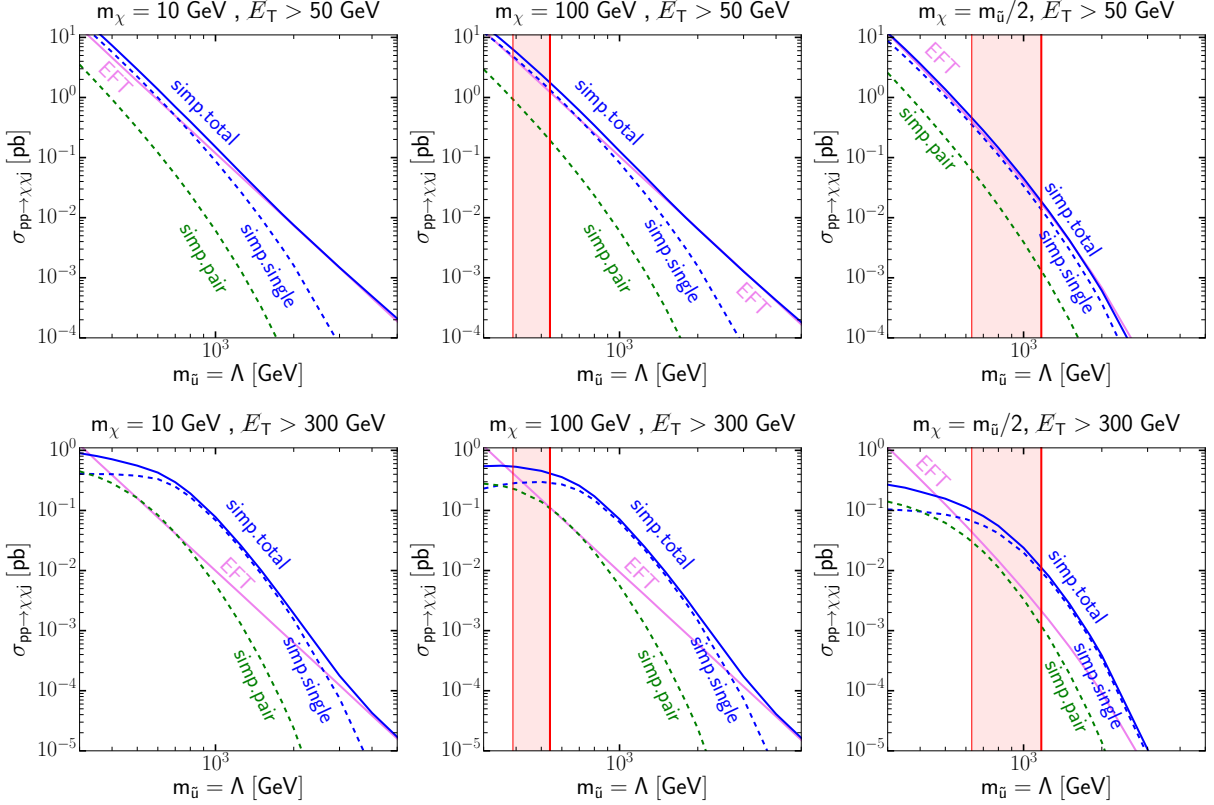


Figure 3. Total production rate in the t -channel model as a function of the mediator mass. The cut on \cancel{E}_T corresponds to a cut on the leading jet at parton level for all processes, except for mediator pair production. The vertical bands show the mediator masses predicting the observed relic density: upper edge for $\Omega_\chi^{\text{obs}} + 10\%$ and lower edge for $\Omega_\chi^{\text{obs}}/3$.

squark. With 20 fb^{-1} data at 8 TeV ATLAS excludes $m_{\tilde{u}} < 470 \text{ GeV}$ for $m_\chi < 100 \text{ GeV}$ [34], comparable to the 13 TeV limits using 3.2 fb^{-1} [35]. For small mass difference between the mediator and the DM particle, there exists an ATLAS mono-jet search which considers pair production in the simplified model and sets a limit $m_{\tilde{u}} \lesssim 260 \dots 300 \text{ GeV}$ for $m_{\tilde{u}} - m_\chi \sim 20 \text{ GeV}$ [36]. Single-resonant or direct $\chi\chi$ production should lead to at least comparable results. Similar limits from CMS rule out $m_{\tilde{u}} < 450 \text{ GeV}$ for $m_\chi < 100 \text{ GeV}$ with 19.2 fb^{-1} at 13 TeV [37]. Mediator masses below 300 GeV are ruled out altogether.

Total rate

One of the key questions in our t -channel model is how the different production mechanisms shown in Fig. 2 decouple towards large mediator masses. First, we study the total production cross section

$$\sigma_{\cancel{E}_T+j}(m_\chi, m_{\tilde{u}}, y_{\tilde{u}}), \quad (18)$$

for fixed dark matter mass and coupling, and as a function of the mediator mass. All our models are implemented in FEYNRULES [32], and we use MADGRAPH5 [38] to compute mono-jet production at the parton level with $|\eta_{j_1}| < 2.5$. Additional QCD jets will not survive the hard analysis cut on $p_{T,j_1} \sim \cancel{E}_T$, except for the specific case of double-resonant mediator pair production. There,

we require the second jet to fulfill $p_{T,j_2} > 20$ GeV, $|\eta_{j_2}| < 4.5$, and $\Delta R_{j_1 j_2} > 0.4$. For illustration purposes our results are based on parton-level simulations. In the appendix we show that using PYTHIA [39] for parton shower and hadronization and DELPHES [40] for the detector simulation, the decoupling patterns remain unchanged.

The panels shown in Fig. 3 include three choices of m_χ combined with two minimum values for the missing transverse energy — at the parton level equivalent to the transverse momentum of the hard jet. The blue solid lines include all Feynman diagrams leading to at least one hard jet, as shown in Fig. 2. For illustration purposes we separate mediator pair production and single-resonant contribution in the ug -initiated sub-process from the continuum process. The regions predicting the correct relic density are also indicated; smaller mediator masses lead to larger annihilation cross section and require another dark matter component, while larger mediator masses require an additional annihilation channel after thermal production.

The different production topologies show a distinctive dependence on the mediator mass. The dependence on the dark matter mass is mild, as long as m_χ does not become too large. For a light mediator both the single-resonant production, and the slightly suppressed pair production, dominate the combined rate. Towards larger mediator masses they decouple more rapidly than the generic t -channel contribution. As a consequence, with only a mild cut $\cancel{E}_T > 50$ GeV the t -channel contribution starts to dominate the total cross section for $m_{\tilde{u}} > 1$ TeV. The crossing point between the two regimes depends on the dark matter mass. Finally, the cross sections show a dependence on the minimum transverse momentum cut. For the simplified model we find that a harder cut on \cancel{E}_T increases the region of mediator masses for which single-resonant production dominates, extending to the multi-TeV mediator regime. We will study the transverse momentum in more detail below.

When the mediator becomes heavy, mono-jet production can be described by an effective Lagrangian including the dimension-6 four-fermion operator,

$$\mathcal{L}_{\text{eff}} \supset \frac{c_{u\chi}}{\Lambda^2} (\bar{u}_R \chi) (\bar{\chi} u_R) . \quad (19)$$

The matching scale is chosen as $\Lambda = m_{\tilde{u}}$, and corresponding to the choice $y_{\tilde{u}} = 1$ we find for the Wilson coefficient $c_{\tilde{u}\chi} = 1$. This operator mediates the t -channel as well as the single-resonant production topologies shown in Fig. 2. In contrast, pair production requires a higher-dimensional operator involving the gluon field strength, like for example

$$\mathcal{L}_{\text{eff}} \supset \frac{c}{\Lambda^3} (\bar{\chi} \chi) G_{\mu\nu} G^{\mu\nu} . \quad (20)$$

This is consistent with its faster decoupling pattern as observed in Fig. 3.

The predictions of the effective Lagrangian in Eq. (19) for the mono-jet rate are also included in Fig. 3. We find good agreement between the effective Lagrangian approximation and the full model even for mediator masses below 1 TeV, as long as the acceptance cut on the transverse momenta is low. This changes when we require globally $\cancel{E}_T > 300$ GeV, i.e. within a factor ten of the mediator mass, motivating a study of the transverse momentum distribution in the mono-jet production process.

Kinematic distributions

For the t -channel mediator model both, the total rate and the kinematic patterns include information about the mediator mass and couplings. To understand the decoupling patterns better we also study the one kinematic observable which we can use to analyze the hard process in mono-jet

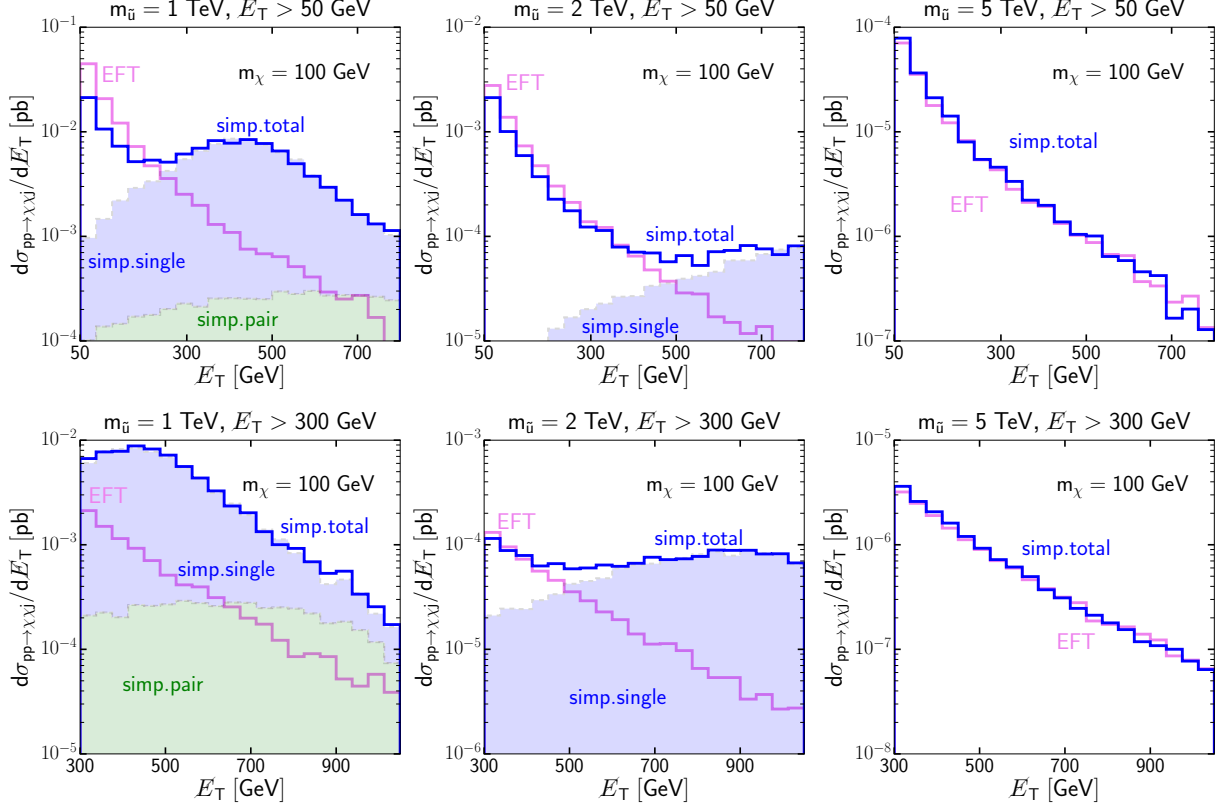


Figure 4. \cancel{E}_T distributions in the t -channel model. The different topologies are stacked to combine to the total rate given in Fig. 3.

production, $\cancel{E}_T \approx p_{T,j_1}$. In Fig. 4 we show stacked histograms for \cancel{E}_T split by tree-level topologies: mediator pair production (dashed green), single-resonant production contribution (dashed blue), and the full mono-jet channel (solid blue), for a selection of $m_{\tilde{u}}$ and m_χ values.

The distributions for a moderate mediator mass of $m_{\tilde{u}} = 1$ TeV are shown in the left panels. Here, the mediator will be copiously produced on-shell, leading to a distinctive \cancel{E}_T dependence: while the resonant contributions peak for large values $\cancel{E}_T \lesssim m_{\tilde{u}}/2$, the generic t -channel contributions prefer low \cancel{E}_T values. Requiring a sizeable \cancel{E}_T then causes a larger reduction of the t -channel cross section, extending the region of dominant resonant production shown in Fig. 3. For larger values of the mediator masses, also shown in Fig. 4, this distinctive t -channel versus resonant cross section behavior is further enhanced. However, given the much faster decoupling pattern of the resonant processes, both the cross section rate and the \cancel{E}_T distribution are eventually dominated by the generic t -channel contributions.

Finally, in Fig. 4 we also show the EFT results, as defined in Eq.(19). Its cross section dependence on \cancel{E}_T is similar to the generic t -channel contributions in the simplified model. The single-resonant contributions are formally included, but implicitly suppressed. Therefore, regardless of the agreement in the inclusive cross section prediction, the EFT will only approximate the \cancel{E}_T distribution of the full model for regions with generic t -channel dominance, *i.e.* in the right panels in Fig. 4. Realistic mono-jet LHC searches require large \cancel{E}_T , pushing the region where the EFT gives a good LHC description to very heavy mediator masses.

Effective Lagrangian vs model

For the t -channel mediator model it only makes sense to study the half plane with $m_\chi < m_{\tilde{u}}$; otherwise the dark matter agent would decay. Because the t -channel mediator carries color charge, LHC constraints typically force us into the regime $m_{\tilde{u}} \gtrsim 1$ TeV. In this situation the dark matter candidate must have a mass at least around 400 GeV, to avoid over-closing the universe; for the same reason the $\tilde{u}-u-\chi$ coupling should be larger than for example in supersymmetric realizations. Both of these requirements point to a valid effective Lagrangian.

One issue with the t -channel model and its effective theory description at moderate mediator masses is the pair production process at the LHC. Because the corresponding production rate does not include any information on the dark sector, an additional branching ratio will only become interesting when we expand the model to allow for two competing decays. However, pair production decouples rapidly with a heavier mediator mass, leading into a regime where single-resonant production plays a more important role. The single-resonant production process is in principle described by the same effective theory as the generic t -channel diagrams. Towards large mediator masses also the single-resonant topology decouples rapidly. Again, this behavior does not signal problems for the effective theory, except for some issues in describing the transverse momentum distributions for still moderate mediator masses.

The key problem of the t -channel model as well as its effective theory is that in the kinematically defined decoupling regime the dark matter annihilation rate and the LHC rates are both small. The model exceeds the measured relic density unless we postulate non-perturbative couplings. Note, however, that this is not a problem caused by the effective Lagrangian. It is a well-known problem with the t -channel mediator model, which for example in supersymmetric models is usually resurrected through co-annihilation. In essence, the effective theory description of the t -channel mediator suffers from many issues of the poorly working full model, leading to a good effective theory approximation only for not very interesting regions of the model parameter space.

III. TREE-LEVEL VECTOR IN S-CHANNEL

An alternative dark matter scenario is a typically fermionic dark matter candidate combined with a s -channel vector mediator V . In supersymmetric models a similar mediator role is played by the Standard Model Z -boson. In general, we need to postulate two interactions,

$$\chi - \chi - V \quad \text{dark matter} \qquad u - u - V \quad \text{Standard Model fermions} . \quad (21)$$

These two couplings induce two competing mediator decays, into Standard Model particles and into dark matter. We assume the mediator to at least couple to quarks in the Standard Model, so we can test the model at the LHC; a tree-level coupling to two gluons becomes a serious issue in setting up the model. There are three different mass regimes in the $m_\chi - m_V$ mass plane,

$$\begin{array}{ll} m_V > 2m_\chi & \text{EFT description possible} \\ m_V \approx 2m_\chi & \text{on-shell} \\ m_V < 2m_\chi & \text{light mediator} . \end{array} \quad (22)$$

This mass relation determines if the generic $2 \rightarrow 2$ process $u\bar{u} \rightarrow \chi\chi$ factorizes into a $2 \rightarrow 1$ kinematics or not. From the LHC perspective the upper two regimes lead to a phase space enhancement. For non-relativistic processes like dark matter annihilation, a phase-space enhancement is limited to the on-shell case. This translates into small couplings predicting the correct relic density, essentially turning off all LHC signatures. For our effective theory considerations at the LHC we will therefore limit ourselves to the first case. The light mediator case is, in general, very interesting because its suppressed $2 \rightarrow 2$ rate will include direct information on both mediator couplings.

We define an overly simple toy model including an s -channel vector to fit our purpose; the mediator V^μ couples only to u -quark pairs and to a dark matter fermion χ ,

$$\mathcal{L} \supset g_u \bar{u} \gamma^\mu V_\mu u + g_\chi \bar{\chi} \gamma^\mu V_\mu \chi . \quad (23)$$

At this stage the mediator does not have any link to the Standard Model gauge groups, but in principle it could. Adding a coupling to d -quarks is trivial. Different observables scale differently with these two couplings,

$$\sigma_{\text{mono-jet}} \propto \frac{g_u^2 g_\chi^2}{\Gamma_V} \qquad \sigma_{\text{resonance}} = \sigma_V \times \frac{\Gamma_{uu}}{\Gamma_V} \propto \frac{g_u^4}{\Gamma_V} \qquad \Gamma_V \sim \Gamma_{\chi\chi} + \Gamma_{uu} . \quad (24)$$

The mono-jet rate can factorize into $\sigma_{V+j} \times \text{BR}_{\chi\chi}$. The di-jet decay signature is essentially limited to the factorized kinematics in the presence of large QCD backgrounds [41]. Throughout our analysis we assume $g_u = g_\chi$, reflecting some kind of comparable charges in the visible and dark sectors. As long as $m_V \gg m_\chi$ this maximizes a potential dark matter signal at the LHC, minimizes the mediator width, and removes the focus from Standard Model resonance searches[†]. On the other hand, such a resonance signal will allow us to extract information from a measurement of $\sigma_{V+j} \times \text{BR}_{uu}$.

The typical total decay width of the mediator becomes

$$\frac{\Gamma_V}{m_V} \lesssim 0.4 \dots 10\% \quad \text{for} \quad g_u = g_\chi = 0.2 \dots 1 , \quad (25)$$

[†] If the LHC should discover a mediator-like resonance without a missing energy signature, an interpretation in terms of dark matter will hardly go beyond the stage of pure speculation.

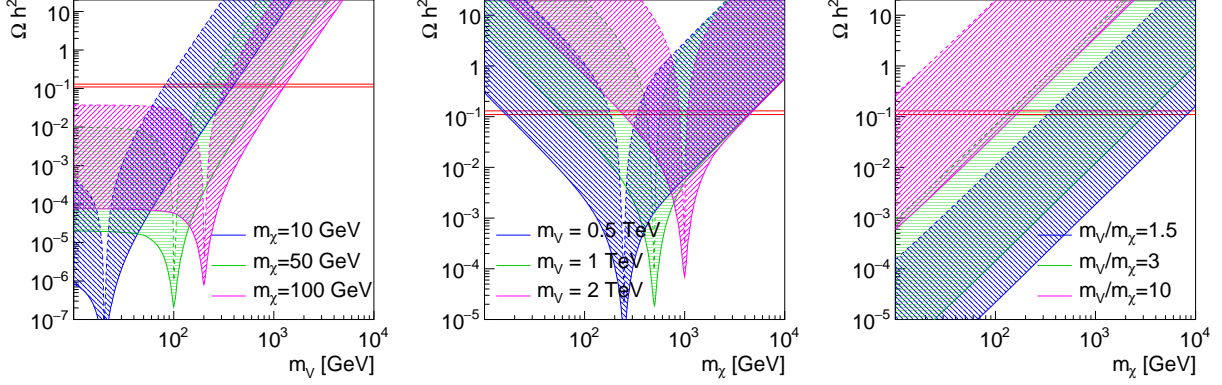


Figure 5. Relic density for the s -channel vector mediator model as a function of the mediator mass for constant dark matter mass (left), as a function of the dark matter mass for constant mediator mass (center) and as a function of the dark matter mass for a constant ratio of mediator to dark matter mass. Over the shaded bands we vary the couplings $g_u = g_\chi = 0.2 \dots 1$; large relic densities correspond to small coupling.

and $m_\chi \ll m_V$. Unlike for the t -channel, the s -channel mediator does not have to be very narrow, in particular if we include additional, flavor-universal couplings. Still, at least for the vector case we do not expect theoretical issues related to an increasing width-to-mass ratio.

As before, we can use the Lagrangian of Eq.(23) to compute the predicted relic density with the help of MICROMEAS. In all three panels of Fig. 5 we observe that for light dark matter the annihilation rate is typically large. Unlike in the t -channel model the predicted relic density easily matches the observed value. In the left panel we can identify the three kinematic regimes defined in Eq.(22): for small mediator masses, $m_V < 2m_\chi$, the annihilation is a $2 \rightarrow 2$ process, but the dependence on the light, off-shell mediator mass is small. For a global analysis of the light-mediator case the non-relativistic annihilation is essentially insensitive to the mediator mass. Around the on-shell condition we can reach the measured relic density with very small couplings, effectively turning off any LHC signature; for heavy mediators the $2 \rightarrow 2$ annihilation process rapidly decouples with large mediator masses. As a side remark, the $\chi - \chi - V$ interaction also introduces a t -channel annihilation $\chi\chi \rightarrow V^*V^*$, but for the vector mediator its contribution is always strongly suppressed by its 4-body phase space.

In the center panel we observe two, almost symmetric solutions in the dark matter mass for a given, large mediator mass. The solution to the right of the pole is hardly consistent with an EFT description, but the solution with $m_\chi < m_V/2$ shows no problems in generating the observed relic density. The limiting factor towards small dark matter masses for example for $m_V = 2$ TeV can be seen in Eq.(2), where the annihilation rate scales with m_χ^2 and should not be too small to predict the correct relic density. In the right panel we focus on mass ratios consistent with an effective theory interpretation and for example find a broad band with $m_V/m_\chi = 10$ and $m_\chi = 10 \dots 100$ GeV with a valid relic density prediction. In this range we also expect a small mediator width $\Gamma_V/m_V \lesssim 10\%$. As for the t -channel model, additional couplings to the full Standard Model fermion spectrum are likely to increase the dark matter annihilation rate by up to an order of magnitude.

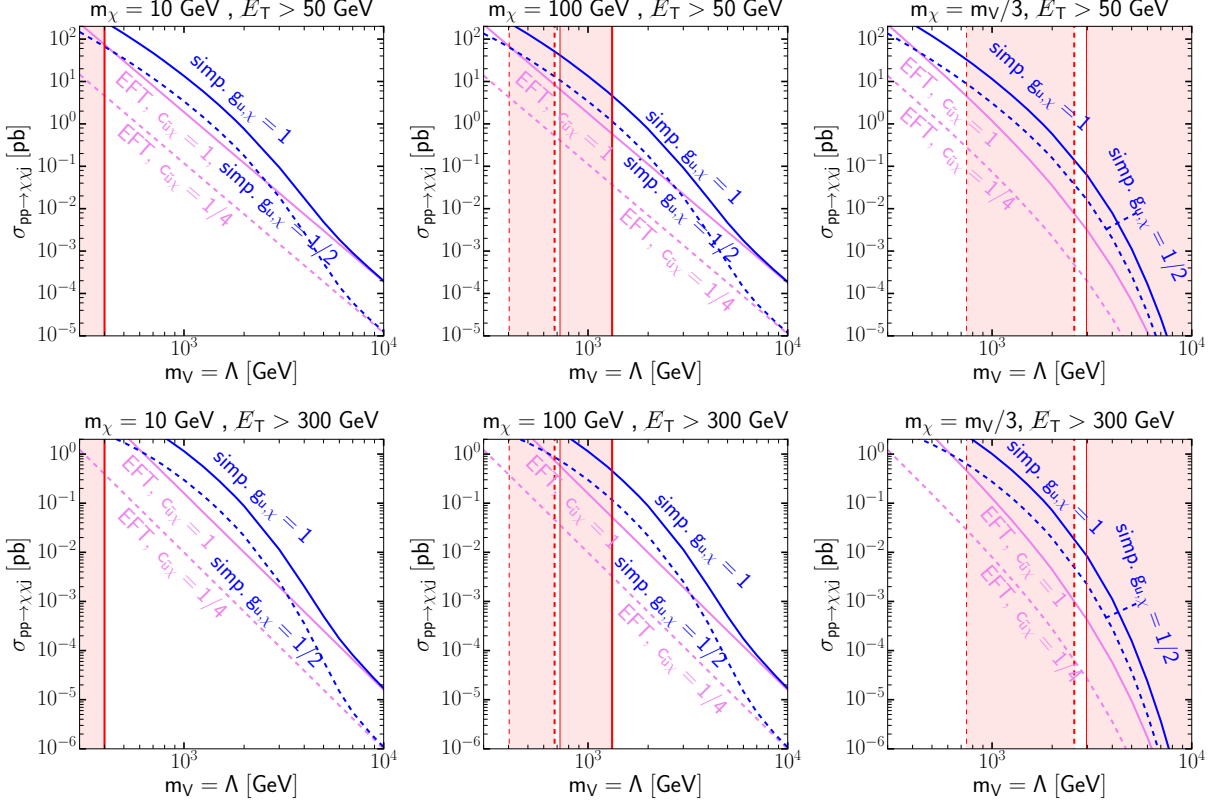


Figure 6. Total production rate in the s -channel vector model as a function of the mediator mass. The cut on \cancel{E}_T corresponds to a cut on the leading jet at parton level. The vertical bands show the mediator masses predicting the observed relic density: upper edge for $\Omega_\chi^{\text{obs}} + 10\%$ and lower edge for $\Omega_\chi^{\text{obs}}/10$.

Total rate

As the first LHC observable we show the total mono-jet production rate for the s -channel vector mediator in Fig. 6,

$$\sigma_{\cancel{E}_T+j}(m_\chi, m_V, g_u = g_\chi). \quad (26)$$

As for the t -channel model we start with a low acceptance cut $\cancel{E}_T > 50$ GeV, where at parton level the hard jet just recoils against the missing momentum. The cut on $p_{T,j}$, correlated with \cancel{E}_T , always regularizes and dials the relative size of σ_{V+j}/σ_V . Because of the final state kinematics, a too stiff cut on $p_{T,j}$ will not allow the mediator to be produced on-shell. This correlation can have a large effect on the cross section after cuts.

The three upper panels of Fig. 6 cover three different dark matter mass values, for mediator masses up to 10 TeV. Following Fig. 5, the heavy mediator regime is consistent with the observed relic density for $m_V/m_\chi \approx 3 \dots 10$ and $g_\chi = g_u = 1$. For a light dark matter candidate with $m_\chi = 10$ GeV the mediator mass corresponding to the observed relic density would be significantly below 1 TeV and likely ruled out by current LHC searches. Heavier mediators are allowed, if there is another dark matter candidate; lighter mediators need another annihilation channel. In addition to the generic case, we also show an alternative, more weakly interacting scenario with $g_\chi = g_u = 1/2$, for which the mediator is clearly a narrow resonance. As expected, the relic density constraint points towards half the mediators mass of the case $g_\chi = g_u = 1$.

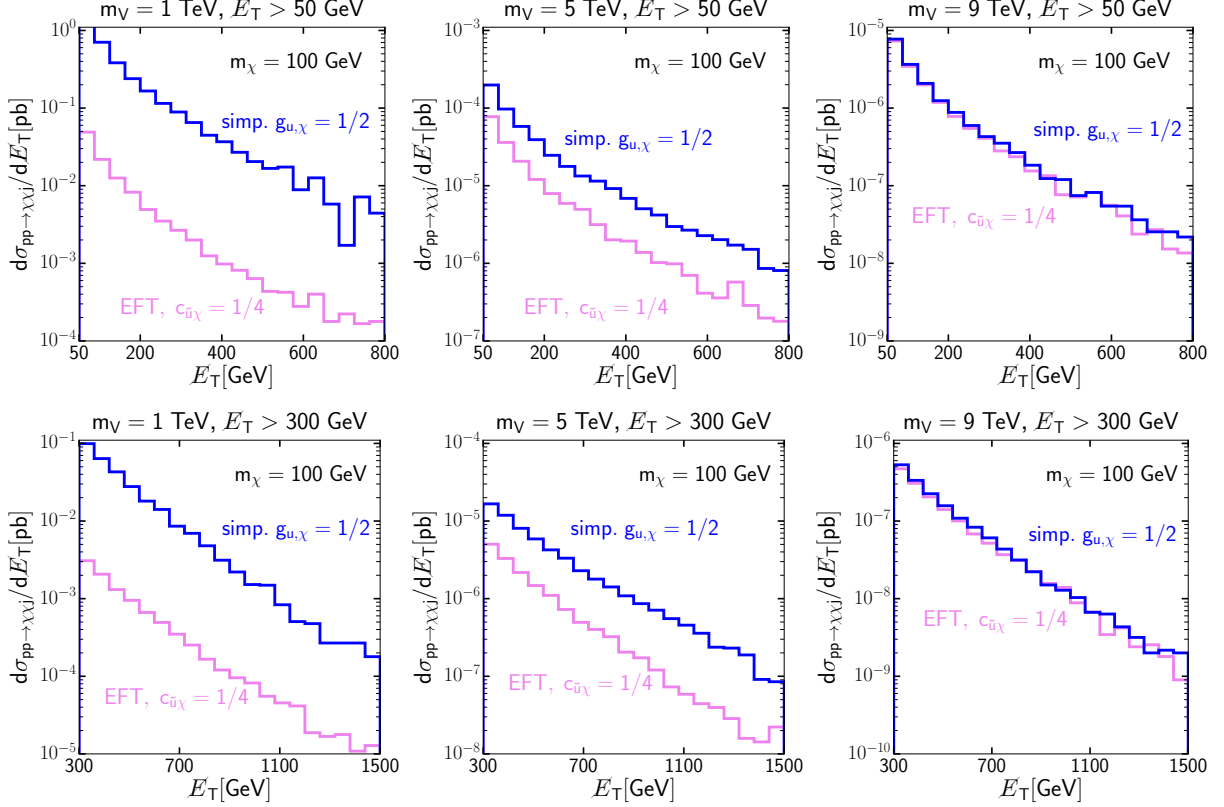


Figure 7. \cancel{E}_T distributions in the s -channel vector mediator model.

The main feature in all curves is that for fixed dark matter masses we observe a change in the scaling of the total rate around $m_V \sim 5$ TeV. At this point the partonic energy scale of the LHC changes the production kinematics from an on-shell mediator production with $\sigma_{\cancel{E}_T+j} = \sigma_{V+j} \times \text{BR}_{\chi\chi}$ to a $2 \rightarrow 2$ description of the hard sub-process $u\bar{u} \rightarrow \chi\chi$ with a decoupled mediator. This change is given by a combination of the proton–proton energy of 13 TeV and the typical momentum fractions of the incoming valence–sea quark pair, and it does not depend on the dark matter model. For example, when we include a stiffer transverse momentum cut of $\cancel{E}_T > 300$ GeV this turn-over point does not move. The main change in the lower panels of Fig. 6 is that the signal rate is suppressed. This suppression is more enhanced for the small mediator masses. Typical mono-jet rates in the heavy-mediator regime can still reach femto-barn cross sections for light dark matter.

Once the s -channel mediator decouples from the mono-jet production process we can describe the model in terms of an effective Lagrangian with the dimension-6 four-fermion operator

$$\mathcal{L}_{\text{eff}} \supset \frac{c_{u\chi}}{\Lambda^2} (\bar{u}\gamma^\mu u) (\bar{\chi}\gamma_\mu \chi) . \quad (27)$$

Matching at $\Lambda = m_V$ gives us a Wilson coefficient $c_{u\chi} = 1$ for $g_\chi = g_u = 1$ and $c_{u\chi} = 1/4$ for $g_\chi = g_u = 1/2$. In Fig. 6 we show the effective Lagrangian predictions for the total LHC rates. As expected, it agrees with the full model predictions in the decoupling region $m_V \gtrsim 5$ TeV. To predict the correct relic density the dark matter candidate should be comparably light, in line with the effective theory requirement. For a constant ratio $m_V/m_\chi = 3$, the agreement of the full model with the effective theory is reached slowly, and it only happens for masses where the LHC rates

are heavily suppressed. In this case, the effective Lagrangian description does never approximate the mono-jet cross section rate well.

Kinematic distributions

In Fig. 7 we show the differential \cancel{E}_T cross section for a selection of dark matter and mediator mass values and for two choices on the \cancel{E}_T cut in the upper and lower panels. We describe the simple, small width scenario with $g_\chi = g_u = 1/2$. The \cancel{E}_T distributions are peaked towards the minimum allowed \cancel{E}_T values and all shown mass values show the same behavior, up to the rate normalization. To allow for an on-shell mediator production we always choose a low acceptance cut on \cancel{E}_T [42].

The normalized distributions for the matched effective operator approximate the simplified model well. The EFT gives a slightly harder distribution for small mediator masses, while it agrees with the full model for heavier mediators. For small mediator masses there exists a difference in the normalization of the total rate, i.e. an EFT interpretation would lead to a wrong measurement of $g_{\chi,u}^2/m_V^2$. This effect is essentially independent of the dark matter mass or the \cancel{E}_T cut, and it poses a major problem for a global EFT analysis. For $m_V \gtrsim 5$ TeV both, the cross section and the differential distributions are in excellent agreement between the full model and the EFT.

Effective Lagrangian vs model

The s -channel vector mediator model can, in principle, cover the entire $m_\chi - m_V$ mass plane. This plane can be separated in to two preferred regimes by the relic density constraints and by the pole condition $m_V/m_\chi = 2$. The half plane with $m_V \lesssim m_\chi$ will not be described by an effective Lagrangian approximation, for $m_V = m_\chi \dots 2m_\chi$ the mediator will stay below its mass shell, but the regime $m_V \gg m_\chi$ can in principle work fine. In the light-mediator case the non-relativistic dark matter annihilation is essentially insensitive to the mediator mass.

The mediator width will be small, as long as we choose the couplings $g_\chi = g_u < 1$. Towards a strongly interacting model it can reach $\Gamma_V/m_V \sim 10\%$, slowly starting to deviate from a narrow resonance description. When we separate the two couplings g_u and g_χ , a smaller value of g_u will suppress the production rate, penalizing the potentially observable LHC mono-jet signatures. The effect of the suppressed cross section is tamed by the increased invisible branching ratio. This way, scenarios with $g_\chi = g_u = 1/2$ will lead to equivalent cross sections as scenarios with $g_\chi = 1$ and $g_u = 1/4$. Conversely, larger values of g_u will allow us to include two-jet resonance searches in a global analysis. In the effective theory's region of validity at the LHC, the mono-jet production rate factorizes into the mediator production rate and the invisible branching ratio. The three ingredients $\sigma_V(m_V, g_u)$, $\Gamma_{\chi\chi}(m_V, m_\chi, g_\chi)$, and $\Gamma_{uu}(m_V, m_\chi, g_\chi)$ have to be combined in a global fit.

The key feature of the effective theory description is that the LHC kinematics introduce another energy scale, namely the maximum amount of partonic energy available to produce a resonance. We find that the mediator turns into a non-propagating state for $m_V \gtrsim 5$ TeV. This value is largely independent of the \cancel{E}_T cut, as well as the specific dark matter mass, as long as $m_V > m_\chi$. This limits the region of validity for a proper effective theory description to a region with very small LHC cross sections. The effect of our relic density constraint is that for very heavy mediators the dark matter particle cannot be too light, either. In essence, the EFT description does not hold in the two regions we are interested in at the LHC: light mediators for $m_V < 2m_\chi$ and moderately heavy mediators with $m_V > 2m_\chi$ but $m_V < 5$ TeV.

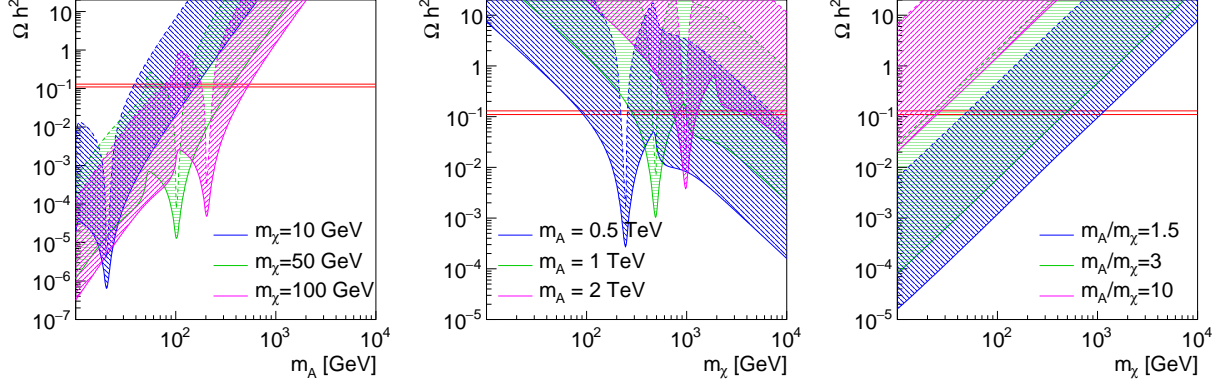


Figure 8. Relic density for the s -channel axial-vector mediator model as a function of the mediator mass for constant dark matter mass (left), as a function of the dark matter mass for constant mediator mass (center) and as a function of the dark matter mass for a constant ratio of mediator to dark matter mass. We assume $g_u = g_\chi = 0.2 \dots 1$; large relic densities correspond to small coupling.

Axial-vector case

We can also assign axial-vector interactions rather than vector interactions to the s -channel mediator,

$$\mathcal{L} \supset g_u \bar{u} \gamma^\mu \gamma^5 A_\mu u + g_\chi \bar{\chi} \gamma^\mu \gamma^5 A_\mu \chi . \quad (28)$$

The preferred region by the observed relic density is given in Fig. 8, indicating that the model can easily reproduce the observed relic density for a wide range of parameters, not just around the pole $m_A \approx 2m_\chi$.

The total and differential rates are shown in Fig. 9. We see literally no change compared to the vector case in Fig. 6 and Fig. 7. The only difference is that the preferred parameter choices for the relic density are shifted. Moreover, the different combinations of vector and axial-vector couplings make a difference in direct detection (constraints), because of different coherent vs incoherent scattering on the nucleus. The axial-vector coupling couples to the spin of the nucleon, there is no coherent enhancement for large nuclei, and the direct detection constraints are significantly weakened. In other words, vector mediator models which are ruled out by direct detection constraints can survive with an axial-vector mediator. For the LHC this assignment makes no difference.

The effective Lagrangian corresponding to Eq.(28) again includes a four-fermion operator,

$$\mathcal{L}_{\text{eff}} \supset \frac{c_{u\chi}}{\Lambda^2} (\bar{u} \gamma^\mu \gamma^5 u) (\bar{\chi} \gamma_\mu \gamma^5 \chi) . \quad (29)$$

As for the vector mediator case the crucial question for the effective theory is if the mediator can be produced as a propagating state, i.e. if $m_V < 5$ TeV.

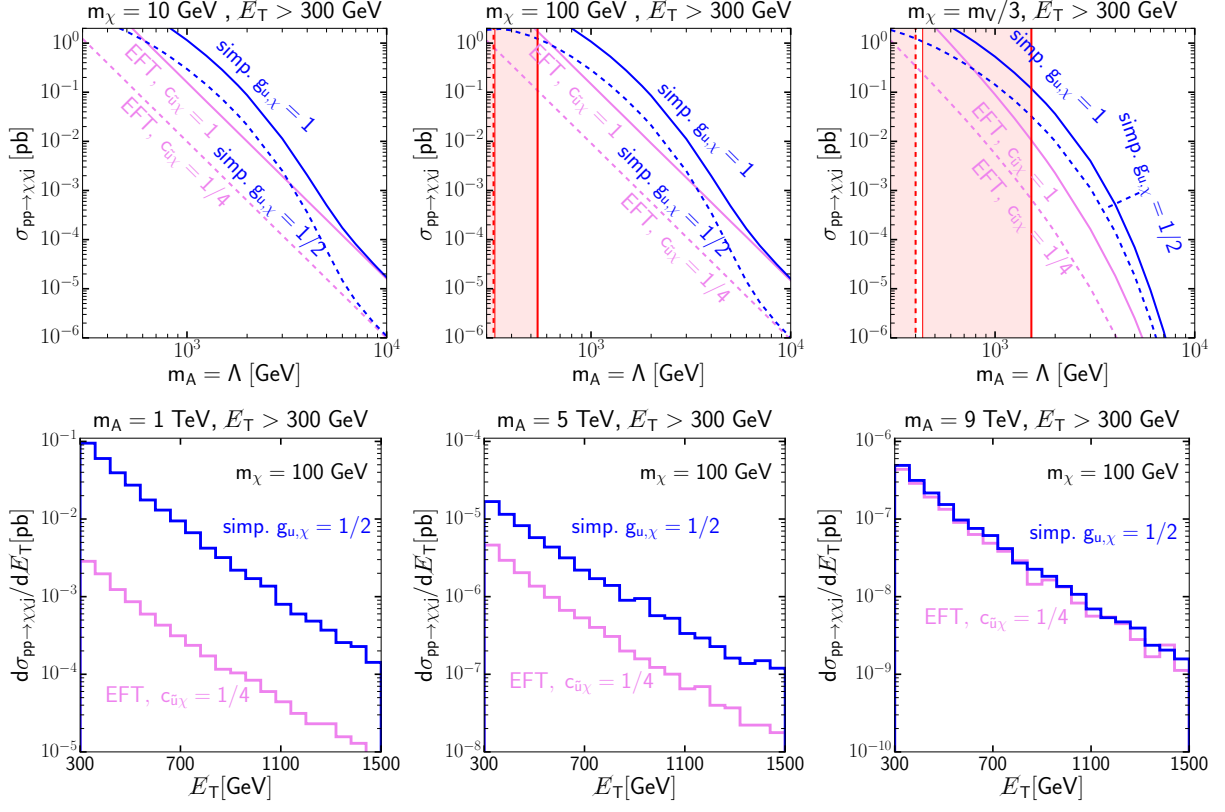


Figure 9. Total production rate (upper panels) and E_T distributions (lower panels) in the s -channel vector mediator model. The vertical lines indicate the mediator masses predicting the observed relic density. The vertical bands show the mediator masses predicting the observed relic density: upper edge for $\Omega_\chi^{\text{obs}} + 10\%$ and lower edge for $\Omega_\chi^{\text{obs}}/10$.

IV. LOOP-MEDIATED SCALAR IN S-CHANNEL

For a (pseudo-)scalar s -channel mediator the situation becomes more complicated. In this case, flavor bounds require minimal flavor violating couplings, resulting in dominant couplings to heavy quarks. A supersymmetric UV-completion includes the heavy (pseudo-)scalar Higgs and neutralino dark matter. As usual, we need to postulate two interactions,

$$\chi - \chi - S \quad \text{dark matter} \quad t - t - S \quad \text{top quarks} . \quad (30)$$

This assumption already reflects the fact that for many reasons we want to avoid introducing very large Yukawa couplings of the new scalar to light quarks. Couplings which are not aligned with the SM Yukawa couplings induce FCNCs, which are lead to strong bounds from flavor observables [19–22, 43]. We therefore allow also for a $c - c - S$ coupling; we will see that it induces the leading dark matter annihilation channel, but have no effect on the LHC signatures. Minimally flavor-violating couplings are automatically realized if we assume a mixing of the SM singlet mediator with the SM Higgs through a portal coupling [24]. Alternative realizations include a singlet coupling to the Standard Model through dimension-5 operators [44], or a $SU(2)_L$ doublet mediator in the case of singlet-doublet dark matter. For the mass spectrum we can distinguish the same three cases as for the vector mediator, Eq.(22). For our EFT analysis at the LHC we will eventually focus on the parameter region

$$m_S > 2m_\chi \quad \text{and} \quad m_S > 2m_t . \quad (31)$$

If we remain agnostic about the underlying theory leading to minimal flavor violation, we can define our toy Lagrangian with the Yukawa interaction

$$\mathcal{L} \supset -\frac{m_t}{v} S \bar{t}(g_{S,t} + i \gamma_5 g_{P,t})t + S \bar{\chi}(g_{S,\chi} + i \gamma_5 g_{P,\chi})\chi + \text{h.c.} \quad (32)$$

We only write out the mediator coupling to top quarks, but we will also study the impact of light-quark couplings to the mediator in a minimal flavor violation structure. The ansatz of the top Yukawa coupling proportional to m_t/v bears no physical relevance, in general it is likely to be suppressed by a new physics scale $\Lambda > v$. The scalar coupling to the dark matter fermions can be linked to m_χ , but does not have to. The partial width of the scalar mediator decaying to top quarks increases with the scalar mass, just like for the Higgs case,

$$\frac{\Gamma_{S \rightarrow tt}}{m_S} = \frac{3G_F m_t^2 g_{S,t}^2}{4\sqrt{2}\pi} \left(1 - \frac{4m_t^2}{m_S^2}\right)^{3/2} < \frac{3G_F m_t^2 g_{S,t}^2}{4\sqrt{2}\pi} < 5\% , \quad (33)$$

assuming $g_{S,t} < 1$. A lighter mediator just decaying to bottom quarks and dark matter would be significantly more narrow, unless we introduce even larger Yukawa couplings than to the top quark, or we couple the scalar to the gauge sector.

Just as for the vector mediator, the mono-jet rate in our parameter region will factorize into $\sigma_{S+j} \times \text{BR}_{\chi\chi}$. Like the Higgs, a light scalar mediator will dominantly be produced through a top-loop-induced coupling to gluons, with an additional gluon jet giving the mono-jet signature. For the Higgs, the corresponding dimension-6 operator does not decouple with the top mass, but is instead suppressed by the electroweak VEV.

As usual, we use the Lagrangian of Eq.(32) to compute the predicted relic density with the help of FEYNRULES[32] and MICROMEGAS[33]. What distinguishes this model from the two models discussed before is that the dark matter annihilation process is not directly related to the LHC production process. Three dark matter annihilation channels are illustrated in Fig. 10. A very

light mediator will decay to two gluons through a top loop. To avoid strong flavor constraints, a tree-level amplitude $\chi\chi \rightarrow c\bar{c}$ will dominate for slightly heavier dark matter and a light mediator. Based on the same couplings, there is a t -channel diagram with a decay to four fermions. If there also exists a Yukawa coupling to bottom quarks, the annihilation of a slightly heavier mediator will then take over as $\chi\bar{\chi} \rightarrow b\bar{b}$. An even heavier mediator will annihilate into off-shell top quarks, $\chi\bar{\chi} \rightarrow (W^+b)(W^-\bar{b})$, and for $m_\chi > m_t$ the simple annihilation process $\chi\bar{\chi} \rightarrow t\bar{t}$ will lead to a very efficient annihilation. In the latter two cases, the link between the LHC production rate and the dark matter annihilation rate becomes very model dependent.

In Fig. 11 we show the predicted relic density for a range of dark matter and mediator masses for scalar and pseudoscalar mediators. The coupling $c - c - S$ with the s -channel (pseudo-)scalar and t -channel dark matter exchange dominates over the process $\chi\bar{\chi} \rightarrow gg$, which we nevertheless include in our numerical analysis. We see two major structures in the mediator mass dependence of the relic density. First, there is the usual peak for non-relativistic annihilation at $m_S = 2m_\chi$, which appears exactly as for a tree-level s -channel vector. In addition, the predicted relic density rapidly drops around $m_S = m_\chi$. The reason for this rapid increase in the annihilation rate is the t -channel diagram $\chi\chi \rightarrow S^*S^*$. It allows for a mass insertion, covering all possible helicity combinations and therefore dominating over the velocity-suppressed s -channel diagram. For the pseudoscalar this velocity suppression is absent, and the peak is less pronounced. This additional diagram makes it easy to match the observed relic density over wide range of dark matter and mediator masses, easier than for example for the s -channel vector case.

The variety of dark matter annihilation channels in our model is not reflected at the LHC. First, the tree-level couplings to charm and top quarks are only relevant for alternative mediator decays. The dominant production process

$$gg \rightarrow S + \text{jets} \rightarrow \chi\bar{\chi} + \text{jets} \quad (34)$$

will introduce the mono-jet signature through initial-state radiation. The corresponding Feynman diagram is shown in the left panel of Fig.10. This process is very well known from Higgs physics, including the phase space region with sizeable jet recoil momentum [45].

Total rate

We implement the loop-mediated s -channel mediator model, as well as its EFT approximations, in FEYNRULES [32] and simulate the mono-jet signal with MADGRAPH5 [38]. For our toy model we show the total rates for $\chi\bar{\chi} + j$ at parton level in Fig. 12. We choose a range of mediator masses of $m_S = 10 \dots 10^5$ GeV, dark matter masses of $m_\chi = 10, 100$ and 200 GeV, and an acceptance cut $E_T > 100$ GeV, translating at parton level into $p_{T,j} > 100$ GeV. Just as for the tree-level s -channel mediator we observe a distinct change in the mediator mass dependence around $m_S = 5$ TeV. Below this transition point the mediator is produced as a propagating degree of freedom and the

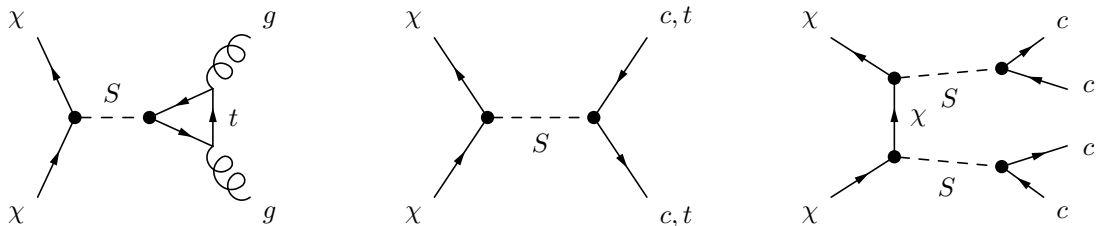


Figure 10. Feynman diagrams describing dark matter annihilation in the scalar s -channel mediator model defined in Eq.(32).

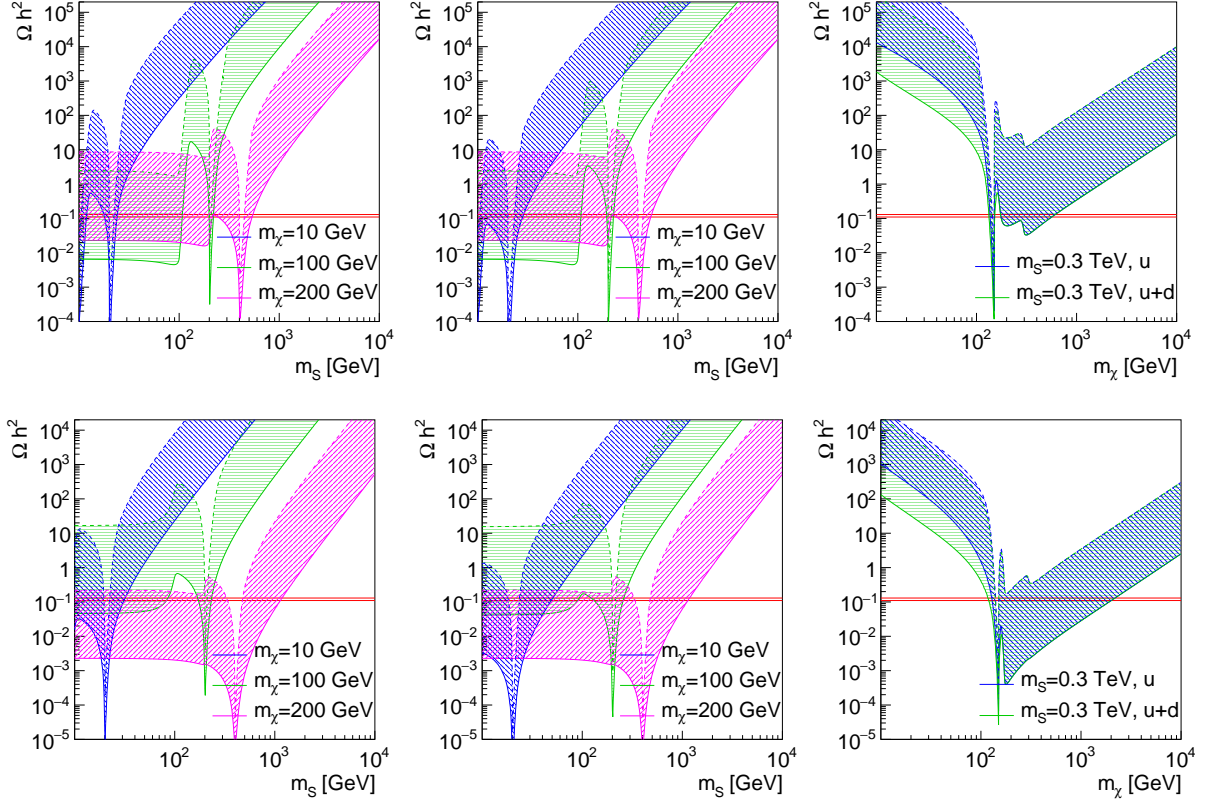


Figure 11. Relic density for the loop-induced s -channel scalar (upper panels) and pseudo-scalar (lower panels) mediator model as a function of the mediator mass for constant dark matter mass with only couplings to up-type quarks (left), with couplings to up- and down-type quarks (center) and as a function of the dark matter mass for a constant mediator mass (right). Over the shaded bands we vary the couplings $g_{S,t} = g_{S,\chi} = 0.2 \dots 1$; large relic densities correspond to small coupling.

mono-jet rate factorizes into $\sigma_{S+j} \times \text{BR}_{\chi\chi}$. Heavier mediators cannot be produced on-shell, leading to the simple scaling $\sigma_{\cancel{E}T+j} \propto 1/m_S^4$. Interestingly, this transition point is almost identical for the $q\bar{q}$ -induced processes and gg -induced processes at the LHC.

Depending on the mass spectrum of our model we can define and match different effective Lagrangians, which can describe the LHC signal more or less reliably [46]. The light dark matter obviously has to remain a propagating degree of freedom. For mediator masses

$$m_t > m_S > 2m_\chi \quad (35)$$

we can — in analogy to the Higgs case — decouple the top quark only, leading to the Lagrangian

$$\mathcal{L}_{\text{eff},1} \supset \frac{c_S^g}{\Lambda} S G_{\mu\nu} G^{\mu\nu} + \frac{c_P^g}{\Lambda} S G_{\mu\nu} \tilde{G}^{\mu\nu} - [S \bar{\chi}(g_S^\chi + i\gamma_5 g_P^\chi)\chi + \text{h.c.}] \quad (36)$$

The Wilson coefficients can be determined at $\Lambda = m_t$

$$\begin{aligned} \frac{c_S^g}{\Lambda} &= \frac{\alpha_s}{8\pi} \frac{g_S^t}{v} \tau [1 + (1 - \tau)f(\tau)] & \xrightarrow{\tau \rightarrow \infty} & \frac{\alpha_s}{12\pi} \frac{g_S^t}{v} \\ \frac{\tilde{c}_P^g}{\Lambda} &= \frac{\alpha_s}{8\pi} \frac{g_P^t}{v} \tau f(\tau) & \xrightarrow{\tau \rightarrow \infty} & \frac{\alpha_s}{8\pi} \frac{g_P^t}{v} \end{aligned} \quad (37)$$

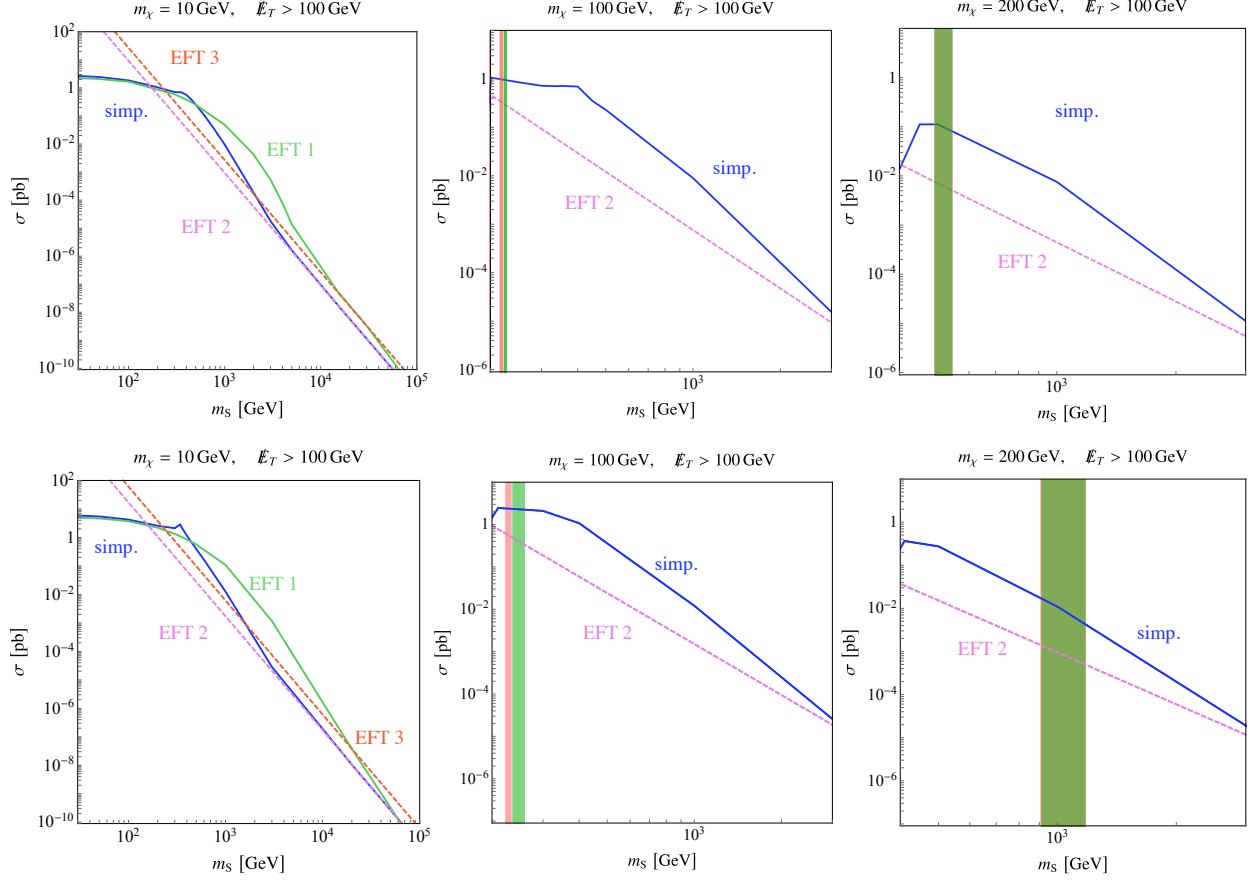


Figure 12. Total production rate in the loop-mediated s -channel scalar model as function of the mediator mass for scalar (upper panels) and pseudoscalar couplings (lower panels). We show all three different effective Lagrangians motivated by different parameter ranges for $m_\chi = 10$ GeV and the most relevant models for $m_\chi = 100$ GeV and 200 GeV. For the red (green) shaded regions the annihilation cross section reproduces the observed relic density within $\Omega_\chi^{\text{obs}}/3$ and $\Omega_\chi^{\text{obs}} + 10\%$.

where $f(\tau) = \arcsin(1/\sqrt{\tau})$ and $\tau = 4m_t^2/m_S^2$. The only difference between this model and the Higgs case is that the effective theory in the Higgs sector is formulated in terms of doublets, leading to dimension-6 operators. We know that in this effective theory the transverse momentum spectra will fail to reproduce large logarithms of the type $\log(p_T/m_t)$ [20, 45], limiting the agreement between the full model and the EFT approximation.

Alternatively, we can follow our original assumption in Eq.(31) and decouple the mediator assuming

$$m_S > m_t, 2m_\chi. \quad (38)$$

We are left with dimension-6 four-fermion operators coupling to the resolved top loop,

$$\mathcal{L}_{\text{eff},2} \supset \frac{c_S^t}{\Lambda^2} (\bar{t}t) (\bar{\chi}\chi) + \frac{c_P^t}{\Lambda^2} (\bar{t}\gamma_5 t) (\bar{\chi}\gamma_5 \chi). \quad (39)$$

The Wilson coefficients after matching at $\Lambda = m_S$ are by

$$\frac{c_S^t}{\Lambda^2} = \frac{g_S^t g_S^\chi}{m_S^2} \frac{m_t}{v} \quad \text{and} \quad \frac{c_P^t}{\Lambda^2} = \frac{g_P^t g_P^\chi}{m_S^2} \frac{m_t}{v}. \quad (40)$$

By definition, this effective theory will retain all top mass effects in the kinematic distributions. Moreover, it ensures that the mediator–gluon coupling is only generated through the top loop and this way allows for a firm link of the LHC observables to the dark matter annihilation process.

Finally, we can brute-force decouple the top quark as well as the scalar mediator

$$m_S \sim m_t > 2m_\chi . \quad (41)$$

If we decouple both of them in one step we find

$$\mathcal{L}_{\text{eff},3} \supset \frac{c_\chi^g}{\Lambda^3} (\bar{\chi}\chi) G_{\mu\nu} G^{\mu\nu} + \frac{\tilde{c}_\chi^g}{\Lambda^3} (\bar{\chi}\gamma_5\chi) G_{\mu\nu} \tilde{G}^{\mu\nu} . \quad (42)$$

The effective operators are dimension-7, *i.e.* further suppressed. Matching at $\Lambda = m_S \sim m_t$ gives us

$$\begin{aligned} \frac{c_\chi^g}{\Lambda^3} &= \frac{\alpha_s}{8\pi} \frac{c_S^t}{\Lambda^2} \frac{1}{m_t} \tau [1 + (1 - \tau)f(\tau)] & \xrightarrow{\tau \rightarrow \infty} & \frac{\alpha_s}{12\pi} \frac{c_S^t}{\Lambda^2} \frac{1}{m_t} = \frac{\alpha_s}{12\pi} \frac{g_S^t g_S^\chi}{m_S^2} \frac{1}{v} \\ \frac{\tilde{c}_\chi^g}{\Lambda^3} &= \frac{\alpha_s}{8\pi} \frac{c_P^t}{\Lambda^2} \frac{1}{m_t} \tau f(\tau) & \xrightarrow{\tau \rightarrow \infty} & \frac{\alpha_s}{8\pi} \frac{c_P^t}{\Lambda^2} \frac{1}{m_t} = \frac{\alpha_s}{8\pi} \frac{g_P^t g_P^\chi}{m_S^2} \frac{1}{v} . \end{aligned} \quad (43)$$

In principle, this model allows for additional particles contributing to the effective mediator–gluon coupling. In our case we fix the limit of the loop-function such that only the top quark runs in the loop.

We show the mono-jet production rates for all three effective Lagrangians in Fig. 12. As expected, the decoupled top ansatz in Eq.(36) reproduces the total rate of the simplified model only if $m_S < 2m_t$. Above that threshold, it overestimates the simplified model cross section, because the $\tau \rightarrow \infty$ limit of the loop function is always larger than its actual value. The effective Lagrangian with the decoupled mediator, Eq.(39), reproduces the dynamic model for $m_S \gtrsim 5$ TeV. Above this value the LHC energy is not sufficient to produce the mediator on-shell. Finally, the effective Lagrangian of Eq.(42) with a simultaneously decoupled top and mediator does not reproduce the total production rate of the simplified model anywhere[‡]. In the center and right panels of Fig. 12, we show the total cross section for heavier dark matter candidates as well as the windows in parameter space for which the annihilation cross section reproduces between one third and 110% of the measured relic density. We show scenarios where the mediator only couples to up-type quarks (shaded red) and where the mediator also couples to down-type quarks (shaded green). For $m_\chi = 200$ GeV, these regions almost completely overlap.

As a side remark, for very large mediator masses the effective Lagrangian with a decoupled top, Eq.(36), fails to precisely reproduce the simplified model prediction. The reason is the mass dependence of the mediator width in the heavy top approximation,

$$\Gamma_S > \Gamma_{S \rightarrow gg} = \frac{2m_S^3}{\pi} \frac{(c_S^g)^2}{\Lambda^2} = \frac{2m_S^3}{\pi} \left(\frac{\alpha_s}{12\pi} \frac{g_S^t}{v} \right)^2 . \quad (44)$$

Clearly, the large mediator mass regime violates the original assumption $m_t \gg m_S$.

[‡] An observed agreement of the full model and this effective theory would correspond to a precise measurement of the mediator mass.

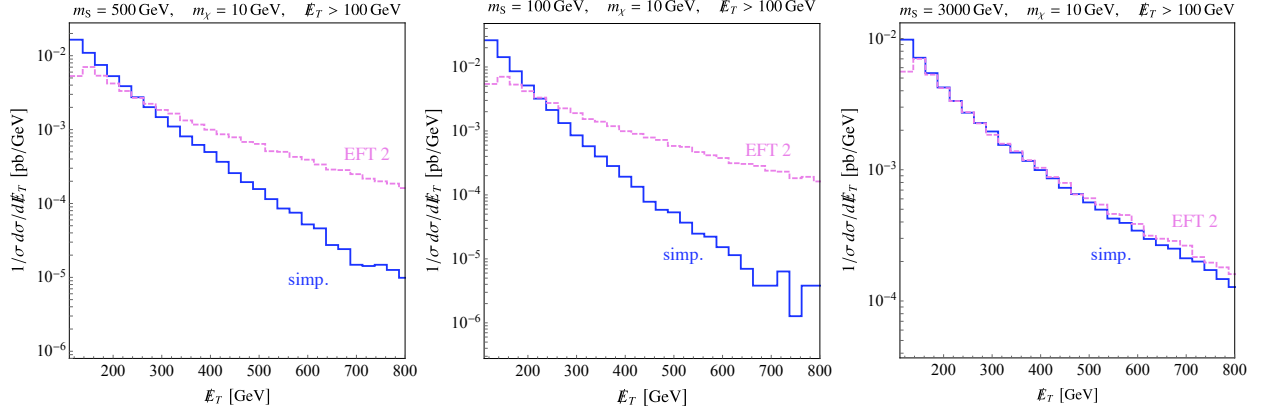


Figure 13. \cancel{E}_T distributions in the loop-induced s -channel scalar mediator model.

Kinematic distributions

In a second step, we consider the normalized \cancel{E}_T distributions. Figure 13 shows this distribution for $m_\chi = 10$ GeV and three mediator masses, $m_S = 100, 500$ and 3000 GeV, based on the simplified model and the effective Lagrangian of Eq. (39) with a decoupled mediator. The couplings are chosen as $g_S^t = g_S^\chi = 1$ in all cases, and we require $\cancel{E}_T > 100$ GeV. Heavy mediators lead to harder p_T spectra. Correspondingly, the EFT spectrum is harder than the simplified model for light mediator masses, becoming indistinguishable for large mediator masses. Since the dominant $Z_{\nu\nu} + \text{jets}$ background is softer than the signal, the signal over background ratio for light mediators suffers from an aggressive \cancel{E}_T cut. For masses $m_S > 2m_t$, searches for a di-top resonance are a promising way to identify an s -channel mediator with dominant couplings to top quarks.

Effective Lagrangian vs model

If a scalar s -channel mediator is predominantly coupled to up-type quarks, the link between the LHC production rate and the predicted relic density essentially vanishes. The two processes, and direct detection limits, are only related if the mediator is very light and hence decays through the one-loop diagram to a pair of gluons. However, this is not the regime where an EFT description with a decoupled mediator should be considered. In this most interesting regime we should decouple the top quark in the loop and keep the mediator and the dark matter agent as propagating degrees of freedom. The features and eventually the failure of this effective theory is well known from the Higgs sector [20, 45].

At the LHC, the assumption of a heavy mediator becomes numerically accurate for $m_S > 5$ TeV, the same way as it does for s -channel mediators produced in quark-antiquark scattering at tree level. This is where an EFT approximation of the mono-jet rate and distributions becomes accurate. The dark matter annihilation process in the early universe is $\chi\bar{\chi} \rightarrow t\bar{t}$, and it can be large around the pole $m_S \approx 2m_\chi$. Because of this effective $2 \rightarrow 1$ annihilation topology, the mediator coupling or mediator decay to Standard Model particles does not play a numerically relevant role. A simultaneous decoupling of the top and the mediator leads to a dimension-7 operators, which we find to be valid nowhere in model parameter space for LHC physics or for dark matter annihilation.

Independent of the EFT description we find that a loop-induced scalar mediator is especially well-suited to explain the observed relic density. The reason is that the t -channel annihilation $\chi\bar{\chi} \rightarrow SS$ does not have the velocity suppression or the $2 \rightarrow 2$ annihilation process.

V. LOOP-MEDIATED SCALAR IN T-CHANNEL

Finally, we consider a scalar t -channel mediator with couplings only to the top quark. This combines some features discussed in Sec. II with Sec. IV. Such a scenario is for example realized by a light scalar top partner in supersymmetry. The relevant interactions are

$$t - \tilde{t} - \chi \quad \text{dark matter annihilation} \quad \tilde{t} - \tilde{t} - g(-g) \quad \text{QCD} , \quad (45)$$

the first of which can lead to decay of $\chi \rightarrow \tilde{t}t^{(*)}$. The condition for stable dark matter, including multi-body decays via an off-shell top and an off-shell W -boson, then reads

$$m_\chi < m_{\tilde{t}} . \quad (46)$$

The second interaction in Eq.(45) occurs through the QCD part of the covariant derivative. The mediator will also have Z and γ interactions from the covariant derivative, but we assume them to be sub-leading at the LHC. In our simplified model the dark matter interaction is described by

$$\mathcal{L} \supset y_{\tilde{t}} (\bar{t}_R \chi) \tilde{t} + \text{h.c.} \quad (47)$$

In contrast to the loop-induced s -channel scalar, couplings to a single quark flavor do not lead to problems with flavor observables, so we assume no interactions between dark matter and light quark flavors.

Dark matter annihilation in this last model proceeds through the tree-level and one-loop diagrams shown in Fig.14. In the regime $m_\chi > m_t$ the annihilation rate is dominated by the tree-level process $\chi\bar{\chi} \rightarrow t\bar{t}$. For $m_\chi < m_t$ annihilation can proceed through off-shell tops with up to a $2 \rightarrow 6$ topology, or the loop-mediated process $\chi\bar{\chi} \rightarrow gg$. In Fig. 15, we present the regions of parameter space for which this mediator can lead to the correct relic density for mediator and dark matter masses above the top threshold. We find that there is a sizeable parameter range for sub-TeV dark matter and mediators where we recover the observed relic density from annihilation into top quarks.

Total rate

As above, we implement the simplified model with FEYNRULES [32] and produce mono-jet events with MADGRAPH5 [38]. At the one-loop level we evaluate around 150 Feynman diagrams, because many internal and external lines in Fig. 14 can radiate a gluon. The total cross section $\sigma_{\cancel{E}T+j}$ is shown in Fig. 16 for mediator masses of $m_{\tilde{t}} = 10 \dots 10^5$ GeV, a dark matter mass of $m_\chi = 10$ GeV,

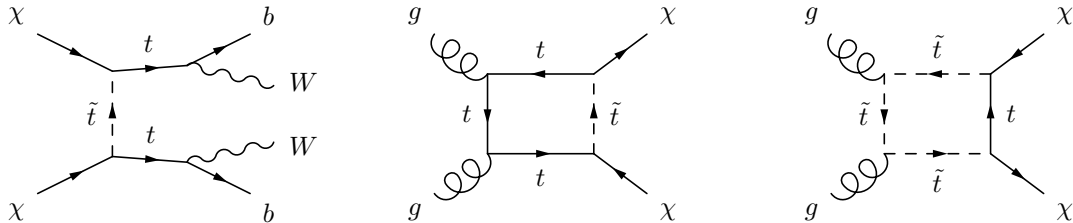


Figure 14. Feynman diagrams describing dark matter annihilation and LHC production (center and right) in the loop-induced scalar t -channel mediator model defined in Eq.(47). Mono-jet production arises from attaching gluons to any of the colored particles.

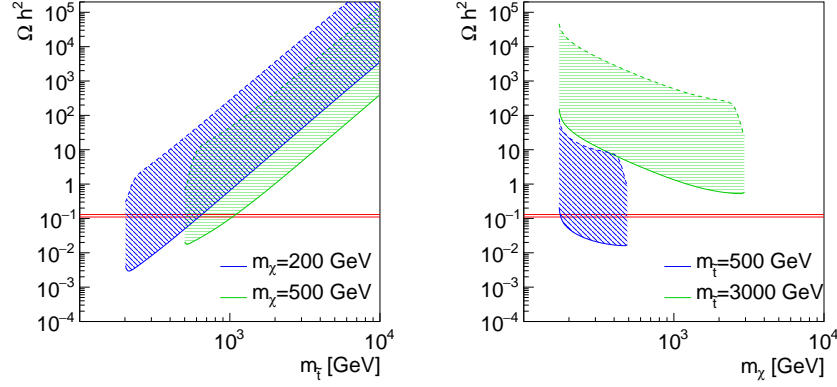


Figure 15. Relic density for the loop-induced t -channel scalar mediator model as a function of the mediator mass for constant dark matter mass (left), as a function of the dark matter mass for constant mediator mass (center) and as a function of the dark matter mass for a constant ratio of mediator to dark matter mass. Over the shaded bands we vary the couplings $g = 0.2 \dots 1$; large relic densities correspond to small coupling.

and a cut $\cancel{E}_T > 100$ GeV. The effective field theory for heavy mediators $m_{\tilde{t}} \gg m_\chi (\sim m_t)$ includes the dimension-6 four-fermion operator,

$$\mathcal{L}_{\text{eff}} \supset \frac{c_{\tilde{t}\chi}}{\Lambda^2} (\bar{t}_R \chi) (\bar{\chi} t_R) , \quad (48)$$

where $\Lambda = m_{\tilde{t}}$ and $c_{\tilde{t}\chi} = 1$ after matching to Eq.(47).

The mono-jet process for this specific model is mediated at one loop in both the simplified model and the EFT. Similar to tree-level t -channel mediator, we again show the pair production rate for the t -channel mediator, with a subsequent decay $\tilde{t}\tilde{t}^* \rightarrow t\bar{t} + \cancel{E}_T$. It occurs at tree level and

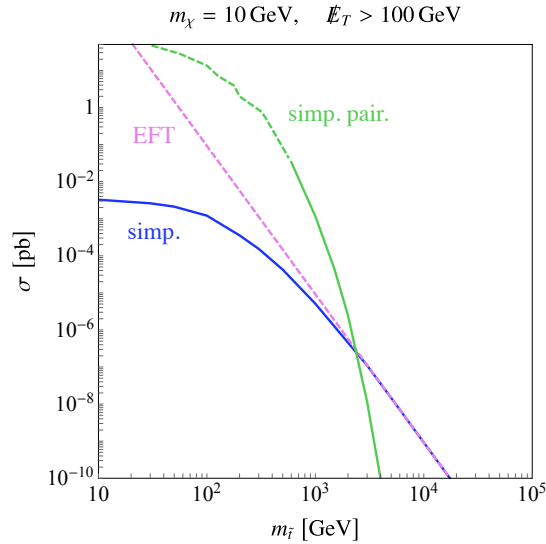


Figure 16. Cross sections for the loop-mediated t -channel scalar model and its effective Lagrangian approximation for the mono-jet signals, and the pair production cross section with subsequent decay into $X + \cancel{E}_T$.

cannot be described by the same effective theory. As a consequence, pair production dominates the LHC signal up to very large mediator masses $m_{\tilde{t}} > 3$ TeV. Here, the mono-jet signal becomes competitive because of the $1/m_{\tilde{t}}^8$ suppression of the pair production rate.

This defines the mass scale where the EFT in principle becomes trustworthy, but where all LHC signals are tiny. It is apparent that the mono-jet cross section in the EFT always overestimates the cross-section predicted by the simplified model, in contrast to the tree-level t -channel mediator discussed in Sec. II. The reason for this is the absence of an s -channel-enhanced diagram like the one in the center of Fig. 2.

When the mediator is below the threshold to allow on-shell $t + \chi$ decays, three body decays into $b + W + \chi$ are considered and similarly four body decays below the W threshold. This region is shown as the green-dashed line in Fig. 16. The requirement of large missing energy reduces the efficiency resulting in a plateau in the $\chi\bar{\chi} + X$ cross section as mediator mass becomes small even if the pair-production cross section is large. ATLAS and CMS searches currently place upper limits on $m_{\tilde{t}}$ in the range of 350..800 GeV depending on m_χ and $m_{\tilde{t}} - m_\chi$.

Effective Lagrangian vs model

If we couple a scalar t -channel mediator only to the top quark, we avoid the associated production which dominates the LHC signal for the usual scalar t -channel mediator. Flavor constraints do not force us to also include Yukawa couplings to light quarks. Dark matter annihilation then proceeds to a variety of channels, including tree-level off-shell processes and loop-induced $2 \rightarrow 2$ topologies. The dominant annihilation mainly depends on the dark matter mass and only slightly on the mediator mass.

In contrast, the decoupling pattern of the LHC rates is largely described by an increasing mediator mass. For relatively light mediators LHC production is dominated by mediator pair production, which is not linked to the leading four-fermion operator as the mono-jet signature or most annihilation channels. On the other hand, in the absence of an associated production channel the effective theory replicates the cross section of the simplified model already for $m_{\tilde{t}} > 3$ TeV. This regime is nevertheless not the most interesting, because the predicted LHC rates are very small.

The mono-jet cross section for a t -channel mediator with couplings to top quarks has the unique property that the EFT always overestimates the prediction in the simplified model due to the absence of any s -channel contribution with resonant enhancement. It reproduces the behavior of the sub-leading t -channel diagrams shown to the left in Fig. 2 for the tree-level t -channel mediator.

VI. SUMMARY

We have studied the performance of an effective field theory of dark matter, focusing on the link between the mono-jet signature at the LHC and the observed relic density. While a link between direct detection and LHC physics is easier to establish [3], the relic density is the most constraining ingredient of any global dark matter fit; a correct description of the main features in the relevant parameter space is crucial for global fits of dark matter in this framework. Our analysis is based on four simple models: a t -channel (darkoquark) mediator; an s -channel vector mediator with tree-level couplings to a dark matter fermion and the Standard Model; and an s -channel or t -channel scalar mediator, coupled to the Standard Model at one loop.

A t -channel scalar mediator is problematic independent of its effective Lagrangian. It is hard to explain the relic density, avoid LHC constraints, and predict measurable LHC signals at the same time. Because LHC prefer heavy mediators, the EFT approximation works fine, including intermediate on-shell states, but it fails to describe appreciable rates at the LHC. An interesting decoupling aspect that the dominant LHC process switches from resonant mediator pair production to single-resonant associated production, to dark matter continuum production with initial state radiation. Note that for the LHC analysis the dark matter mass plays hardly any rule, except for degenerate dark matter and mediator scenarios which cannot be linked to the relic density.

The s -channel vector mediator is interesting because of its resonance structure in non-relativistic annihilation and at the LHC. From a global fit perspective, the factorization into $2 \rightarrow 1$ production and decay matrix elements hurts the parameter analysis hard. By definition, the EFT description works in a different region of phase space. In this case the partonic LHC energy plays a key role; mediator production is described by a propagating mediator up to $m_V \approx 5$ TeV, above which the model merges into an EFT.

The loop-mediated s -channel scalar mediator can be matched it to three effective Lagrangians. Obviously, we need to choose the correct decoupling pattern for valid LHC predictions: a decoupled top quark in the loop-induced gluon-mediator coupling is essentially identical to the low-energy description of Higgs production at the LHC, and it is well known that it should not be applied to hard mono-jet production. A decoupled mediator scenario works well at the LHC, provided the mediator mass exceeds 5 TeV. Decoupling the mediator and the top at the same time does not yield a valid effective theory for the LHC.

For the loop-mediated t -channel scalar mediator there is no associated production of the mediator with dark matter. This means that the appropriate EFT provides a good description already for mediator masses above 3 TeV. In contrast to the tree-level t -channel and the s -channel models, the EFT always overestimates the suppressed mono-jet rate predicted by the full model. This means that the EFT again approximates the full model only in parameter regions where the expected number of events is very small.

A side result of our study is that the relevant energy scales for an EFT description at the LHC are the mediator mass and the partonic LHC energy. The exact mass of the dark matter (away from a degenerate spectrum $m_{\text{med}} \approx m_\chi$) or the mediator width do not play a noticeable role.

Based on our EFT comparison with four typical models we find that a correct description of LHC observables like the total mono-jet rate and the relevant range of the missing transverse momentum spectrum is not actually the main challenge to the EFT framework. From a global fit perspective it is crucial to link the predicted relic density to LHC observables. Unlike the link between mono-jet production and direct detection, this link between mono-jet production and the relic density is not established in our models and does not suggest to perform global fits to an effective theory of dark matter.

Acknowledgments

We are very grateful to the MITP program *Understanding the First Results from LHC Run II* for triggering the questions leading to this paper and for their outstanding hospitality in a great town. A. B. is funded by the *Heidelberg Graduate School for Fundamental Interactions*. All authors acknowledge support from the German Research Foundation (DFG) through the Forschergruppe *New Physics at the Large Hadron Collider* (FOR 2239). ND also acknowledges partial support from the OCEVU Labex (ANR-11-LABX-0060) and the A*MIDEX project (ANR-11-IDEX-0001-02) funded by the *Investissements d'Avenir* program.

Appendix A: Detector effects

Throughout the main body of the paper we show parton level results, *i.e.* one hard jet recoils against the missing energy, $\cancel{E}_T = p_{T,j}$. We keep this choice to be able to illustrate all the sub-channel contributions, their different behavior, and to allow for a comparison between the different models. In this appendix we show the robustness of these results when we include a proper event simulation. Aside from the implementation of the models in FEYNRULES [32] and the generation of events with MADGRAPH[38], we use PYTHIA [39] for parton shower and hadronization, and the default ATLAS setup in DELPHES [40] for the detector simulation. This includes FASTJET [47] for jet clustering. For the event production we generate events including up to two hard jets, plus soft and collinear jet radiation. As for the parton-level results discussed before, we require at least one central hard jet, $|\eta_j| < 2.5$, consistent with the usual mono-jet searches. While after the proper simulation \cancel{E}_T and $p_{T,j}$ are still highly correlated, they are no longer strictly equal. Therefore, we apply a cut on \cancel{E}_T combined with $p_{T,j}^{\text{lead}} > 50$ GeV for the leading jet. This way, the reconstruction corresponds to the usual LHC analyses. Finally, motivated by the mono-jet searches, we veto events with more than two jets with $|\eta_j| < 4.5$ and $p_{T,j} > 30$ GeV.

For illustration purposes it is sufficient to focus on the tree-level t -channel mediator, described in Sec. II. We again set $y_u = 1$, or $c_{u\chi} = 1$ for the EFT approximation. Following the structure of the paper, we start showing total cross sections after the above introduced selection cuts. Given the mild dependence of the cross sections on the dark matter mass, we use $m_\chi = 10$ GeV.

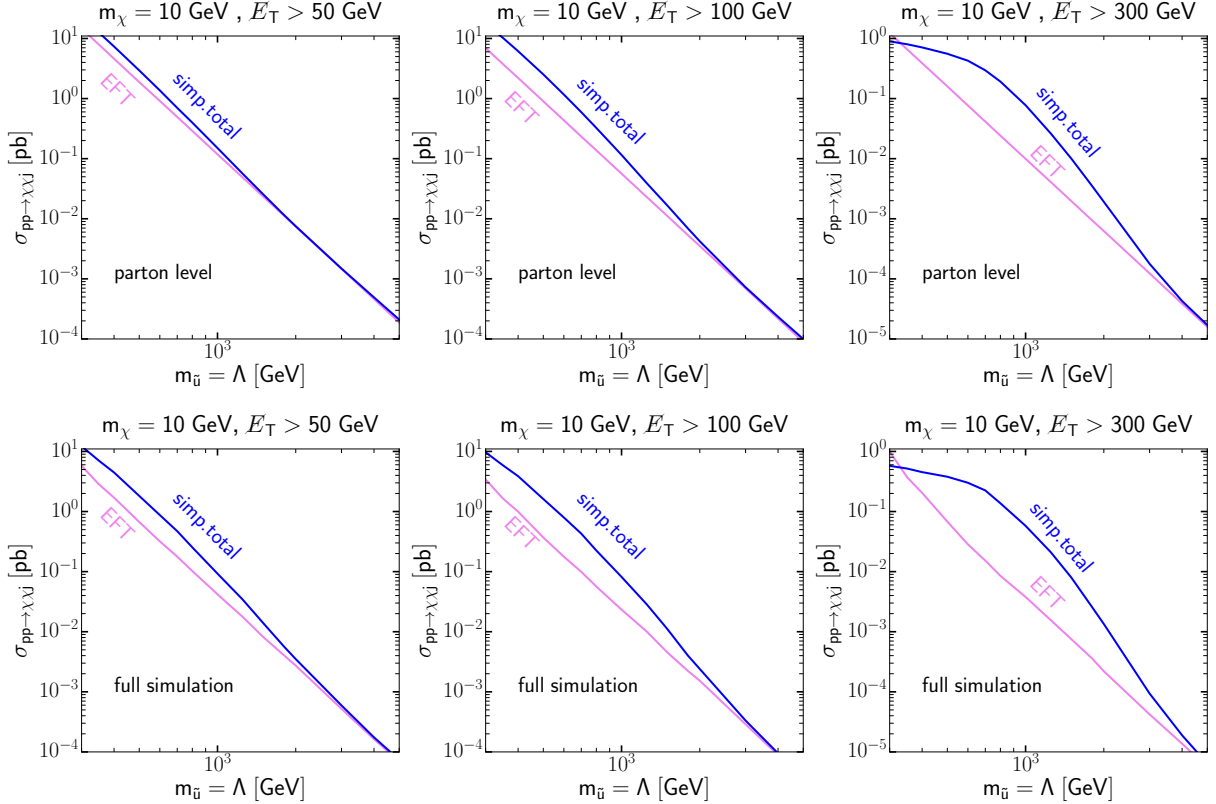


Figure 17. Total production rate in the t -channel model as a function of the mediator mass. In the upper panels we show again the results obtained from the parton level simulations. The lower plots include the full simulation procedure chain.

As can be observed in Fig. 17, all features we describe in Sec. II remain after the proper simulation. Specifically, the decoupling pattern for the simplified model towards the effective Lagrangian is identical. For the smallest and least realistic \cancel{E}_T cut, the agreement between the simplified model cross section and the effective Lagrangian approximation is already accomplished for mediator masses around 1 TeV. A larger cut on \cancel{E}_T delays the decoupling limit to larger mediator masses, rendering the effective Lagrangian approximation valid for multi-TeV mediators. The only differences appearing in the proper simulation are in the precise cross section values. They are reduced compared to parton level; this is caused by the more sophisticated treatment of the detection and reconstruction of the hard jet, as well as of the missing energy. We note here that the precise values for the predicted cross sections will depend on the final requirements imposed on the reconstructed jets, as well as on higher-order corrections.

Finally, even though Fig. 17 already points to unaltered shapes of the \cancel{E}_T distributions, we show a selection of such distributions in Fig. 18. We fix the missing transverse momentum cut to $\cancel{E}_T > 50$ GeV, and we show the distributions for both the simplified model and the effective Lagrangian approximation for $m_\chi = 10$ GeV, and mediator masses $m_{\tilde{u}} = 1, 2$ and 5 TeV.

We see exactly the same patterns as in Sec. II. For the lightest mediator masses considered, $m_{\tilde{u}} = 1$ TeV, the single-resonant diagrams dominate the simplified model cross sections. The \cancel{E}_T distribution in the simplified model is very different from the EFT distribution. The latter has a similar shape as the pure t -channel contributions. For larger mediator masses the impact of the single-resonant channel is reduced. The deviations of the effective Lagrangian from the simplified model are only visible for the larger \cancel{E}_T values. For the largest mediator mass, $m_{\tilde{u}} = 5$ TeV, the

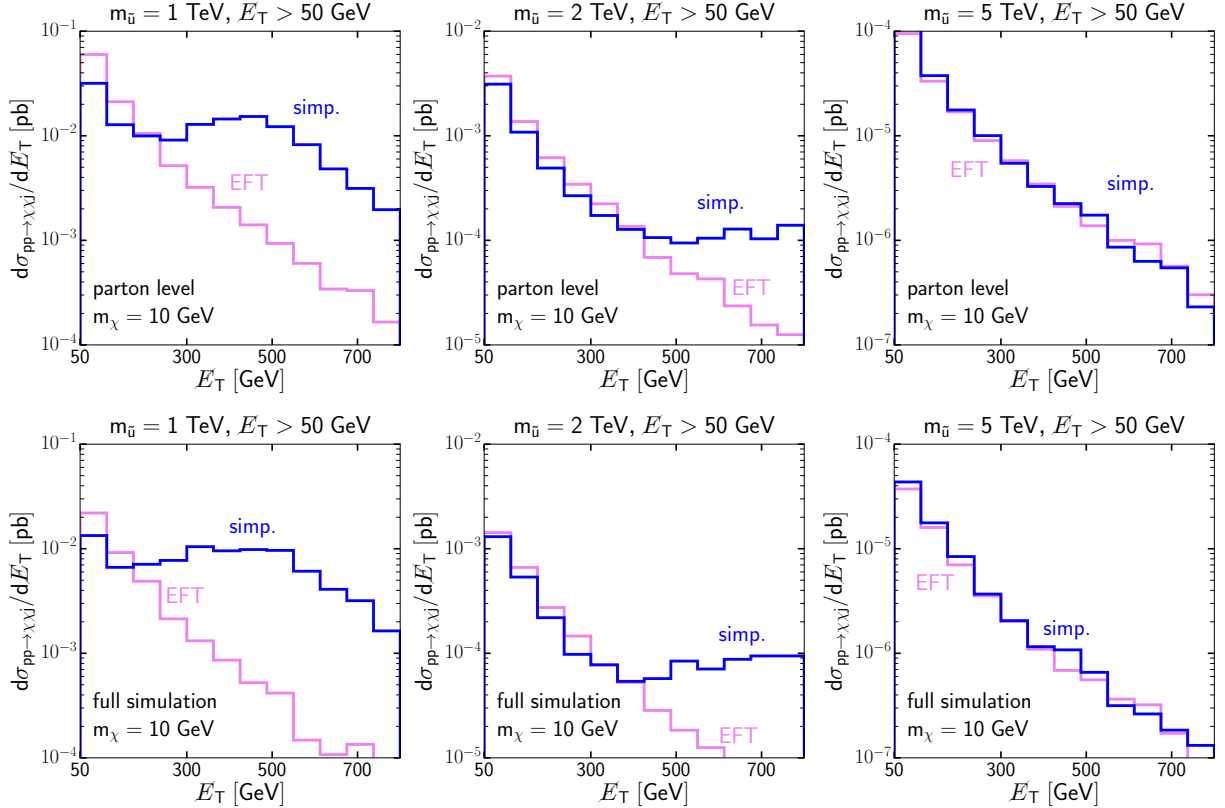


Figure 18. \cancel{E}_T distributions in the t -channel model. In the upper panels we show the results obtained from the parton level simulations. The lower plots depict the distributions after the full simulation procedure.

simplified model and the effective approximations are in full agreement, for the total cross section and for the \cancel{E}_T distribution. Our parton-level simulation in the main body of the paper is entirely justified.

-
- [1] S. Weinberg, Phys. Lett. B **91**, 51 (1980); S. R. Coleman, J. Wess and B. Zumino, Phys. Rev. **177**, 2239 (1969); C. G. Callan, Jr., S. R. Coleman, J. Wess and B. Zumino, Phys. Rev. **177**, 2247 (1969).
 - [2] C. J. C. Burges and H. J. Schnitzer, Nucl. Phys. B **228**, 464 (1983); C. N. Leung, S. T. Love and S. Rao, Z. Phys. C **31**, 433 (1986); W. Buchmüller and D. Wyler, Nucl. Phys. B **268**, 621 (1986); W. Kilian, Springer Tracts Mod. Phys. **198**, 1 (2003).
 - [3] A. Rajaraman, W. Shepherd, T. M. P. Tait and A. M. Wijangco, Phys. Rev. D **84**, 095013 (2011); J. Goodman, M. Ibe, A. Rajaraman, W. Shepherd, T. M. P. Tait and H. B. Yu, Phys. Lett. B **695**, 185 (2011); J. Goodman, M. Ibe, A. Rajaraman, W. Shepherd, T. M. P. Tait and H. B. Yu, Phys. Rev. D **82**, 116010 (2010); J. Goodman, M. Ibe, A. Rajaraman, W. Shepherd, T. M. P. Tait and H. B. Yu, Nucl. Phys. B **844**, 55 (2011).
 - [4] Q. H. Cao, C. R. Chen, C. S. Li and H. Zhang, JHEP **1108**, 018 (2011); S. Chang, R. Edezhath, J. Hutchinson and M. Luty, Phys. Rev. D **89**, no. 1, 015011 (2014).
 - [5] S. Liem, G. Bertone, F. Calore, R. Ruiz de Austri, T. M. P. Tait, R. Trotta and C. Weniger, JHEP **1609**, 077 (2016).
 - [6] Z. H. Yu, J. M. Zheng, X. J. Bi, Z. Li, D. X. Yao and H. H. Zhang, Nucl. Phys. B **860**, 115 (2012); A. De Simone, A. Monin, A. Thamm and A. Urbano, JCAP **1302**, 039 (2013); J. Y. Chen, E. W. Kolb and L. T. Wang, Phys. Dark Univ. **2**, 200 (2013); M. Cannoni, Eur. Phys. J. C **76**, no. 3, 137 (2016).
 - [7] K. Cheung, P. Y. Tseng and T. C. Yuan, JCAP **1101**, 004 (2011); K. Cheung, P. Y. Tseng and T. C. Yuan, JCAP **1106**, 023 (2011).
 - [8] J. Fan, M. Reece and L. T. Wang, JCAP **1011**, 042 (2010); A. L. Fitzpatrick, W. Haxton, E. Katz, N. Lubbers and Y. Xu, JCAP **1302**, 004 (2013); F. Bishara, J. Brod, B. Grinstein and J. Zupan, arXiv:1611.00368 [hep-ph].
 - [9] P. J. Fox, R. Harnik, J. Kopp and Y. Tsai, Phys. Rev. D **85**, 056011 (2012).
 - [10] D. de Florian *et al.* [LHC Higgs Cross Section Working Group Collaboration], arXiv:1610.07922 [hep-ph].
 - [11] G. Busoni, A. De Simone, E. Morgante and A. Riotto, Phys. Lett. B **728**, 412 (2014); G. Busoni, A. De Simone, J. Gramling, E. Morgante and A. Riotto, JCAP **1406**, 060 (2014); G. Busoni, A. De Simone, T. Jacques, E. Morgante and A. Riotto, JCAP **1409**, 022 (2014).
 - [12] S. Bruggisser, F. Riva and A. Urbano, JHEP **1611**, 069 (2016).
 - [13] J. Brehmer, A. Freitas, D. Lopez-Val and T. Plehn, Phys. Rev. D **93**, no. 7, 075014 (2016).
 - [14] J. Ellis, V. Sanz and T. You, JHEP **1503**, 157 (2015).
 - [15] L. Berthier and M. Trott, JHEP **1505**, 024 (2015); L. Berthier and M. Trott, JHEP **1602**, 069 (2016); R. Contino, A. Falkowski, F. Goertz, C. Grojean and F. Riva, JHEP **1607**, 144 (2016).
 - [16] M. T. Frandsen, F. Kahlhoefer, A. Preston, S. Sarkar and K. Schmidt-Hoberg, JHEP **1207**, 123 (2012); H. An, L. T. Wang and H. Zhang, Phys. Rev. D **89**, no. 11, 115014 (2014); N. F. Bell, Y. Cai, J. B. Dent, R. K. Leane and T. J. Weiler, Phys. Rev. D **92**, no. 5, 053008 (2015); A. De Simone and T. Jacques, Eur. Phys. J. C **76**, no. 7, 367 (2016).
 - [17] P. Agrawal, Z. Chacko, C. Kilic and R. K. Mishra, arXiv:1003.1912 [hep-ph]; T. Jacques and K. Nordstrom, JHEP **1506**, 142 (2015) J. Abdallah *et al.*, Phys. Dark Univ. **9-10**, 8 (2015); D. Abercrombie *et al.*, arXiv:1507.00966 [hep-ex]; A. Boveia *et al.*, arXiv:1603.04156 [hep-ex].
 - [18] E. Dudas, Y. Mambrini, S. Pokorski and A. Romagnoni, JHEP **0908** (2009) 014; P. J. Fox, J. Liu, D. Tucker-Smith and N. Weiner, Phys. Rev. D **84** (2011) 115006.
 - [19] U. Haisch, F. Kahlhoefer and J. Unwin, JHEP **1307** (2013) 125; U. Haisch, A. Hibbs and E. Re, Phys. Rev. D **89** (2014) 034009; P. Harris, V. V. Khoze, M. Spannowsky and C. Williams, Phys. Rev. D **91** (2015) 055009; U. Haisch and E. Re, JHEP **1506** (2015) 078.
 - [20] M. R. Buckley, D. Feld and D. Goncalves, Phys. Rev. D **91**, 015017 (2015).
 - [21] O. Mattelaer and E. Vryonidou, Eur. Phys. J. C **75** (2015) no.9, 436.
 - [22] M. J. Dolan, F. Kahlhoefer, C. McCabe and K. Schmidt-Hoberg, JHEP **1503** (2015) 171 Erratum:

- [JHEP **1507** (2015) 103].
- [23] Y. G. Kim, K. Y. Lee and S. Shin, JHEP **0805** (2008) 100; S. Baek, P. Ko and W. I. Park, JHEP **1202** (2012) 047; L. Lopez-Honorez, T. Schwetz and J. Zupan, Phys. Lett. B **716** (2012) 179; M. Fairbairn and R. Hogan, JHEP **1309** (2013) 022.
 - [24] M. Bauer *et al.*, arXiv:1607.06680 [hep-ex].
 - [25] N. F. Bell, J. B. Dent, A. J. Galea, T. D. Jacques, L. M. Krauss and T. J. Weiler, Phys. Rev. D **86** (2012) 096011; S. Chang, R. Edezhath, J. Hutchinson and M. Luty, Phys. Rev. D **89** (2014) no.1, 015011; A. DiFranzo, K. I. Nagao, A. Rajaraman and T. M. P. Tait, JHEP **1311** (2013) 014 Erratum: [JHEP **1401** (2014) 162]; M. Papucci, A. Vichi and K. M. Zurek, JHEP **1411** (2014) 024.
 - [26] N. F. Bell, Y. Cai and R. K. Leane, JCAP **1601** (2016) no.01, 051.
 - [27] U. Haisch, F. Kahlhoefer and T. M. P. Tait, Phys. Lett. B **760** (2016) 207.
 - [28] F. Kahlhoefer, K. Schmidt-Hoberg, T. Schwetz and S. Vogl, JHEP **1602**, 016 (2016).
 - [29] C. Englert, M. McCullough and M. Spannowsky, Phys. Dark Univ. **14** (2016) 48.
 - [30] S. P. Martin and M. T. Vaughn, Phys. Lett. B **318**, 331 (1993).
 - [31] Y. Bai and J. Berger, JHEP **1311**, 171 (2013).
 - [32] A. Alloul, N. D. Christensen, C. Degrande, C. Duhr and B. Fuks, Comput. Phys. Commun. **185**, 2250 (2014); N. D. Christensen and C. Duhr, Comput. Phys. Commun. **180**, 1614 (2009).
 - [33] G. Belanger, F. Boudjema, P. Brun, A. Pukhov, S. Rosier-Lees, P. Salati and A. Semenov, Comput. Phys. Commun. **182**, 842 (2011).
 - [34] G. Aad *et al.* [ATLAS Collaboration], JHEP **1409**, 176 (2014).
 - [35] M. Aaboud *et al.* [ATLAS Collaboration], Eur. Phys. J. C **76**, no. 7, 392 (2016).
 - [36] M. Aaboud *et al.* [ATLAS Collaboration], Phys. Rev. D **94**, no. 3, 032005 (2016).
 - [37] CMS Collaboration, CMS-PAS-SUS-16-014.
 - [38] J. Alwall *et al.*, JHEP **1407**, 079 (2014).
 - [39] T. Sjostrand, S. Mrenna and P. Z. Skands, JHEP **0605**, 026 (2006).
 - [40] J. de Favereau *et al.* [DELPHES 3 Collaboration], JHEP **1402**, 057 (2014).
 - [41] F. Krauss, S. Kuttimalai and T. Plehn, arXiv:1611.00767 [hep-ph].
 - [42] O. Buchmueller, M. J. Dolan and C. McCabe, JHEP **1401**, 025 (2014).
 - [43] P. J. Fox and C. Williams, Phys. Rev. D **87** (2013) no.5, 054030.
 - [44] M. Bauer, A. Butter, J. Gonzalez-Fraile, T. Plehn and M. Rauch, arXiv:1607.04562 [hep-ph].
 - [45] R. K. Ellis, I. Hinchliffe, M. Soldate and J. J. van der Bij, Nucl. Phys. B **297**, 221 (1988); U. Baur and E. W. N. Glover, Nucl. Phys. B **339**, 38 (1990); R. V. Harlander, T. Neumann, K. J. Ozeren and M. Wiesemann, JHEP **1208**, 139 (2012); A. Banfi, A. Martin and V. Sanz, arXiv:1308.4771 [hep-ph]; A. Azatov and A. Paul, JHEP **1401**, 014 (2014); C. Grojean, E. Salvioni, M. Schlaffer and A. Weiler, JHEP **1405**, 022 (2014); M. Buschmann, C. Englert, D. Goncalves, T. Plehn and M. Spannowsky, Phys. Rev. D **90**, 013010 (2014); M. Buschmann, D. Goncalves, S. Kuttimalai, M. Schönherr, F. Krauss and T. Plehn, JHEP **1502**, 038 (2015).
 - [46] for a similar discussion in the Higgs sector see e.g. A. Freitas, D. Lopez-Val and T. Plehn, Phys. Rev. D **94**, no. 9, 095007 (2016).
 - [47] M. Cacciari, G. P. Salam and G. Soyez, JHEP **0804**, 063 (2008); M. Cacciari, G. P. Salam and G. Soyez, Eur. Phys. J. C **72**, 1896 (2012).